consists of four electrically controlled solenoid valves, sample and reference glass containers, plastic pipes, and mass flow controller. Noteworthy, it is necessary for this type of measurement to switch between the reference and the sample glass containers. Four electrically controlled solenoid valves were used to avoid mixing of the gas from the reference and the sample. The gas either from the reference or sample containers was set to flow into the sensor chamber at a flow rate of 150 ml/min. For the measurement circuit, data acquisition was realized by a USB DAQ device (NI USB-6008) from National Instruments where each sensor voltage was measured with a dedicated channel of the DAQ device. The measurement software was written under LabVIEW package. The voltage divider method was employed for measuring the resistance of each sensor. The DAQ device was configured to acquire 2,000 samples at a time with a sampling rate of 2,000 samples per second for each channel. This generates an array of data that spans one second. To obtain noise reduction and higher precision, these 2,000 samples were then averaged to obtain only one value per second per channel. The resulting values were then recorded in a file for subsequent analyses.

In our study, only simple features, i.e., the maximum and minimum resistances as obtained from switching between the reference and sample, were extracted and used for analyses, as shown in Figure 2a. The maximum and minimum resistances were the averaged values of their 10 neighboring data points. Since there is a gradual change in the reference and sample resistances over time, it is necessary to correct such baseline shift as time proceeds (See Figure 2b).

Figure 2. (a) Typical raw data from a sensor and the max/min feature extraction on each curve. (b) Correction method of baseline shift as time proceeds.

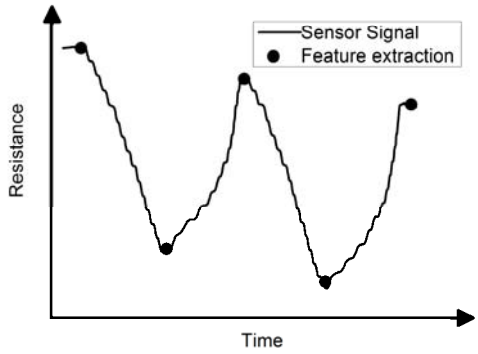

(a)

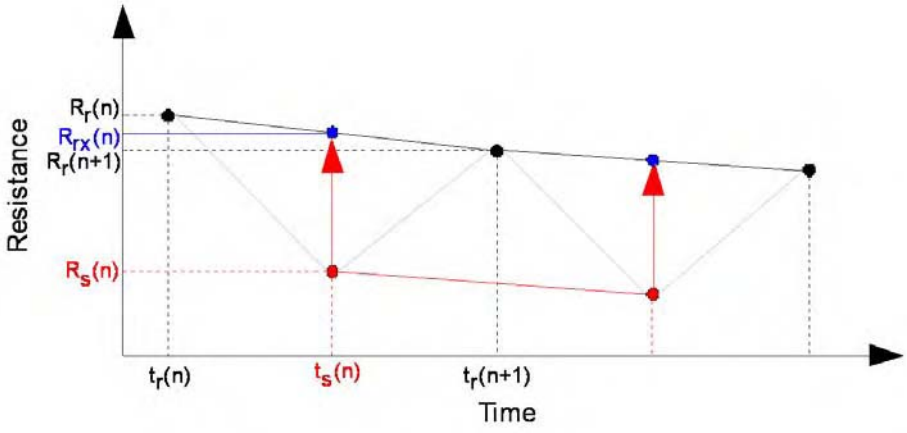

(b)

From Figure 2, index r denotes the reference, while index s denotes the sample. Index rx is defined as a baseline-corrected reference value. The variable (n) represents the running number of measurement loop (switching between the reference and sample). A linear interpolation is used as a baseline connecting between two reference points [$R_r(n)$ and $R_r(n + 1)$]. The corrected reference point [$R_{rx}(n)$] is calculated by projecting the sample point onto the baseline. As a result, the baseline-corrected difference between the sample and reference resistances is calculated via the following formula:

$$\Delta R(n) = R_s(n) - R_{rx}(n) \tag{1}$$

$$\text{Where } R_{rx}(n) = \frac{R_r(n+1) - R_r(n)}{2} + R_r(n) \tag{2}$$

For later data analysis and to compare data of different types of sensors, it is better to calculate the percentage change of resistance:

$$\%R(n) = \frac{R_s(n) - R_{rx}(n)}{R_{rx}(n)} \times 100 \tag{3}$$

Figure 3. Schematic diagram of humidity control using hardware-based method.

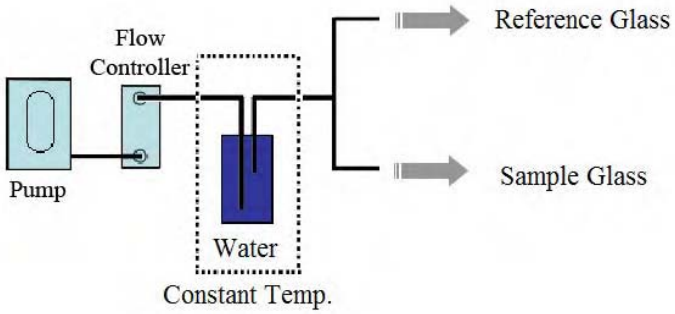

2.2. Humidity Control

As discussed in the introduction, most chemical gas sensors are sensitive to humidity. Therefore, if two identical samples with a different humidity are measured, the results can be different. In our work, we propose two methods as solutions to this problem. The first is a hardware-based method, where the sample was handled so as to have almost the same humidity as the background. Under such condition, the humidity signals will be equivalent for the sample and the reference, thereby only signals from the odors of interest result. To produce a constant humidity background, the carrier gas was directed to flow through a liquid water container that is immersed in a temperature-controlled heat bath (see Figure 3). The temperature of the heat bath can be adjusted until the generated humidity reaches the desired value. It is intuitive to anticipate that the native humidity would be lower than the higher generated humidity. We have done an experiment to investigate whether the generated humidity could overcome the native humidity of the samples. A humidity sensor was installed inside the sensor

chamber. The temperature of the heat bath was adjusted until the reference humidity reached a desired value of 25%, 50% and 75%, respectively. Then, the humidity difference between the reference and the sample was compared and discussed (Section 3.1).

The second solution to the humidity problem is a software-based approach. A mathematical model describing the resistance of each gas sensor at different humidity level can be calibrated to subtract the humidity signal from the total signal. Although each aforementioned approach can be used independently, we have employed both schemes concurrently to achieve maximum accuracy. In addition, it should be noted that these humidity corrections could be applied in other E-nose systems or in the field conditions. Samples other than the human body odor can also be used with this algorithm. However, varying humidity (10–90%) should be tested before a measurement of a desired sample.

2.3. Human Body Odor Collection

Human body odors from armpits were collected from two male volunteers. The experiment was performed for five days with a sample collection of the armpit odors in the morning right after waking up (the volunteers typically wake up around 7–8 am) and in the afternoon (8 hours later). Cotton pads were used to transfer the odors from the armpits to the E-nose. A cotton pad must be in direct contact with the armpit for 10 minutes and stored in a special sample glass bottles with a screw-on closure. Once the morning samples were collected, the glass bottles were transferred to laboratory for E-nose measurement. To minimize the odor change due to bacteria, the samples, transferred via a heat-protection container, were measured within 30–50 minutes after sample collection. For the afternoon samples, E-nose measurement can be done immediately after odor sampling.

During the experiment period, the volunteers were requested to go about their ordinary life and activities: for example, they took a shower twice a day (before going to bed and after waking up following the morning sample collection). To avoid fluctuation in odor samples, they were not allowed to have sex and/or consume alcohol. To study the effects from deodorant, the volunteers were requested to use deodorant, after taking shower in the morning, but only on the right arm.

Table 2. The concentration of the isovaleric acid levels that correspond to subjective impression by using human nose.

Level	Concentration of aqueous isovaleric acid solution (mM)	Subjective impression
0	0	No odor
1	0.12	Slight
2	0.48	Definite
3	1.99	Moderate
4	7.88	Strong
5	32.33	Very strong

2.4. Evaluation of Sensor Response to Body Odor Strength

There are more refined and less subjective ways to measure odor strength in direct way. For instance, the concept of dilution-to-threshold principle can be used quite accurately to reduce uncertainties associated with subjective impressions [30–32]. In the cosmetic industry, human olfaction has been commonly employed to evaluate the odor strength of armpit for the development of deodorants. The armpit odor comprises a complex set of chemicals. Previously, isovaleric acid and volatile steroids (such as androstenone, androstadienone and androstenol) were thought to be the major contributors to armpit odor. However, armpit odor having more distinct and pungent oder involves the presence of other volatile compounds as well [33–35]. To simplify the odor strength of armpit, only a single component such as isovaleric acid can be used for training the sensory panel [36] and representing the sweaty primary odor [37,38] that contributes mainly to the armpit malodor. Hooper *et al* [36,39] assigned the concentrations of isovaleric acid levels on a scale 0 to 5 corresponding to subjective impression by using human nose, as shown in Table 2. Their test was carried out by a team of three female assessors of ages ranging from 20 to 40 years. They were selected for olfactory evaluation on the basis that each person is able to rank correctly the odor levels of the series of aqueous isovaleric acid solution listed in Table 2. The scale 0 to 5 has been usually used to represent the intensity of the armpit smell in the cosmetic industry. The judges are trained to memorize this scale and classify the odor strength of the samples. In this work, we evaluated the performance of E-nose in classification of body odor strength using isovaleric acid solutions prepared according to the intensity scale. A cosmetic face-cleaning pad with 0.15 mL of aqueous isovaleric solution was placed into a glass container for measurement.

3. Results and Discussion

3.1. Humidity Control

To investigate the sensor response to humidity, the relative humidity [%RH] was varied from 30% to 80%. Resistances arisen from humidity of TGS 813, TGS 825, and TGS 2602 sensors are displayed in Figure 4a,b,c, respectively. The graphs for the behaviors of TGS 822 and TSG880 (not shown in this paper) are similar to TGS 813. Mathematical models for the sensors' response to humidity can be fitted via the following formulations:

Exponential equation of TGS 813:

$$Rs_{813} = 86682.00 \exp\left(\frac{-[\%RH]}{29.05}\right) + 55063.48 \tag{4}$$

Exponential equation of TGS 822:

$$Rs_{822} = 24931.58 \exp\left(\frac{-[\%RH]}{37.48}\right) + 9054.41 \tag{5}$$

Exponential equation of TGS 880:

$$Rs_{880} = 90496.88 \exp\left(\frac{-[\%RH]}{36.33}\right) + 55135.22 \quad (6)$$

Polynomial equation of TGS 2602:

$$Rs_{2602} = 6958.22 + 129.172[\%RH] - 0.9788[\%RH]^2 \quad (7)$$

Polynomial equation of TGS 825:

$$Rs_{825} = 5646.63 + 103.26[\%RH] - 1.34[\%RH]^2 \quad (8)$$

Figure 4. Resistance of sensors (a) TGS 813, (b) TGS 825 and (c) TGS 2602 versus relative humidity.

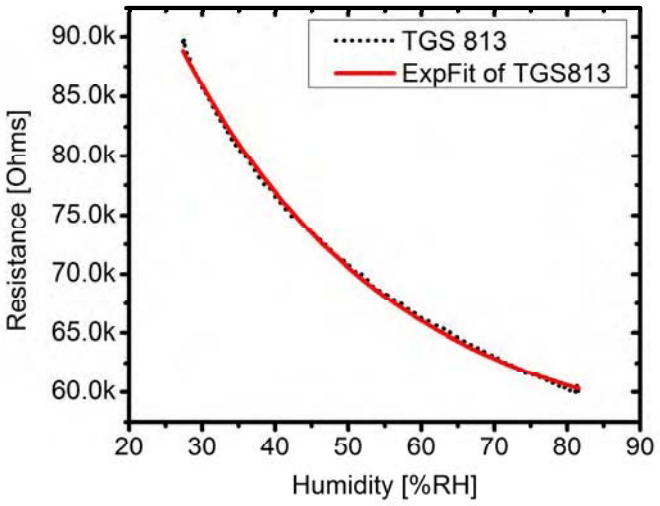

(a)

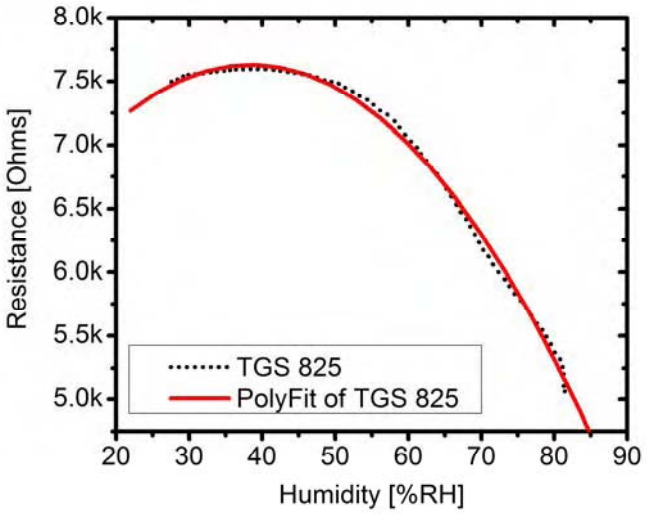

(b)

Figure 4. *Cont.*

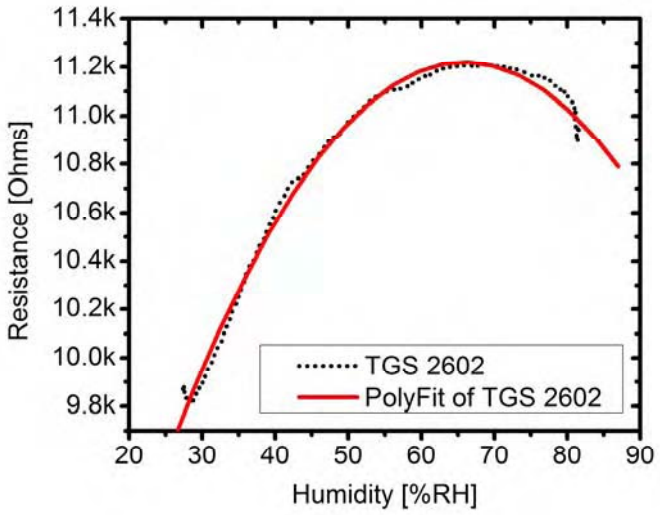

(c)

These mathematical models were included in the data acquisition and analysis codes, thus allowing the response of sensors to humidity of the samples to be corrected on the fly. However, to achieve the maximum accuracy, hardware correction as shown in Figure 3 is co-employed. It was expected that, if the generated background humidity dominates the humidity of the sample, the effect arising from the humidity difference between the reference and the sample would be minimized. We have tested this assumption by measuring the armpit odor sample of a volunteer. Various humidity references, e.g., 25%, 50% and 70%, were generated and flowed through the sample. Table 3 shows absolute average percentage changes of resistances of each sensor and their standard deviations (or standard error) upon varying humidity background. Each average percentage changes of resistance presented in Table 3 was obtained by averaging data from three repeated measurements, in which each measurement performs switching between the reference and sample for five cycles (in total 15 datasets of each sensor were averaged). It was found that the change of the resistance between the reference (pure cotton pad) and the sample (cotton pad + sweat + armpit odor) and its error value become smaller when the background humidity was increased from 25% to 75%. The variation in each measurement, as implied by the standard error, was also reduced from ±51% with low humidity background to ±7% with higher humidity background, indicating that fluctuation in the dynamic measurement was also reduced. The decreasing error indicates less fluctuation of the sensor response arising from the humidity in sweat. At a lower relative humidity, the sweat in the cotton pad can evaporate much easier and contributes in a large part for the difference of resistances between the reference and the sample. At a higher relative humidity, the generated humidity weighs off the native humidity of the sample, thereby reducing the humidity difference between the reference and the sample. As shown on the right-most column of Table 3, the humidity difference between the reference and the sample decrease from 2.8% to only 0.29% when the generated humidity at 25% was replaced by higher relative humidity at 75%. However, saturated humidity (100%) is not recommended because it will suppress evaporation of odor molecules, which deteriorates the measurement.

The hardware-based method helps to reduce the effect arising from the humidity reference between the reference and the sample. It can be said that the sensor signals consist in a large part of the contribution from the odors of interest. Thus, relative humidity at 75% was applied in all experiments for measuring the human body odors in this paper.

Table 3. The absolute average percentage change of resistance of each sensor upon varying humidity generated by hardware correction.

Background humidity	TGS813	TGS825	TGS2602	TGS880	TGS822	Humidity sensor
25%	3.948 (±55%)	2.211 (±38%)	3.727 (±38%)	4.765 (±37%)	5.529 (±43%)	2.823 (±51%)
50%	0.526 (±16%)	0.104 (±23%)	0.264 (±27%)	0.702 (±25%)	2.150 (±25%)	0.550 (±20%)
75%	0.158 (±4%)	0.057 (±8%)	0.581 (±4%)	0.160 (±5%)	0.185 (±7%)	0.293 (±7%)

3.2. Evaluation of Sensor Response to Body Odor Strength

The response of each sensor to the isovaleric acid prepared according the intensity levels 1 to 5 is displayed in Figure 5. It can be seen that all sensors can discriminate intensity level 3, 4 and 5, but fail to distinguish between levels 0, 1 and 2. TGS2602 exhibits the highest response to the isovaleric acid. Since the intensity level of isovaleric acid has an exponential relation with the concentration (as seen in Table 2), the sensor response may be mathematically adjusted in order to understand the relationship between the sensor response with the intensity level, using the logarithmic function:

$$Y = \ln(1 - \%R_S) \tag{9}$$

Figure 5. (a) Sensor response to isovaleric acid at different intensity level. (b) Logarithmic plot of the sensor response.

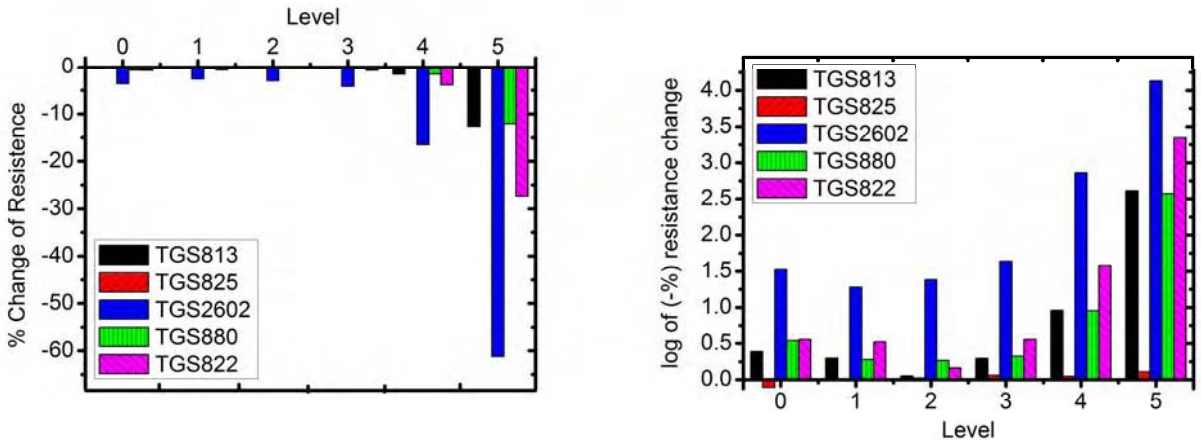

(a) (b)

As shown Figure 5b, the logarithm of sensor response is linear with the odor strength for the intensity levels 3–5. The intensity threshold to isovaleric acid for all sensors is the intensity level 3.

It implies that our E-nose may be limited to classify odor strength of persons who have at least definite armpit smell. Therefore, we have chosen two volunteers who have moderate armpit odors for E-nose measurement.

3.3. Detection and Classification of Human Body Odor

Armpit odors of two volunteer persons were measured by an E-nose during five days using a combined hardware/software humidity correction. Figure 6a,b exhibits the average of sensor response over 5 days as measured on the left (denoted by L) and right (denoted by R) armpits.

Figure 6. The sensor response with error bar of (a) person A and (b) person B in the morning and the afternoon. L and R denote the left and right armpits, respectively.

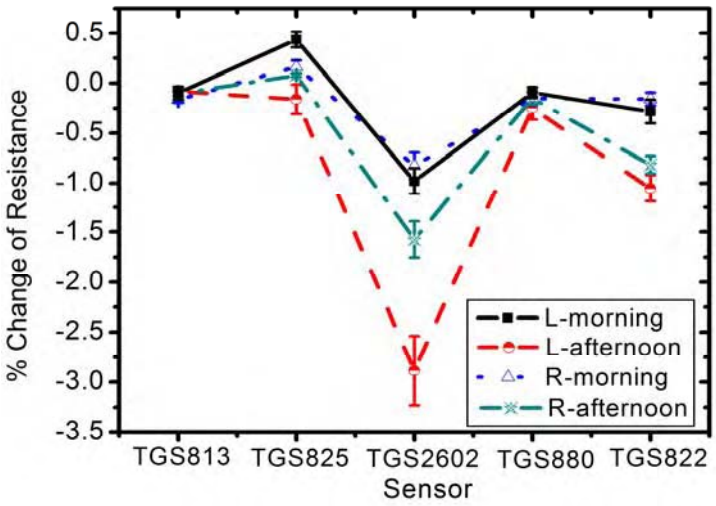

(a)

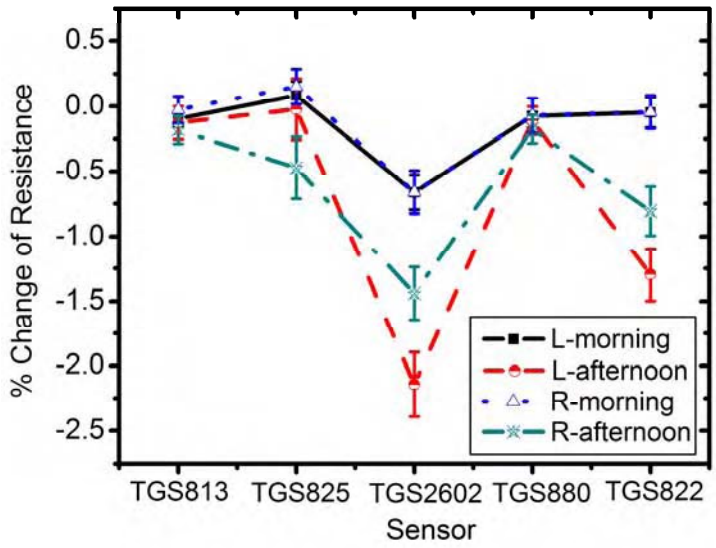

(b)

From Figure 6, it was found that TGS822 and TGS2602 have a high response to human body odor, in agreement with previous tests with isovaleric acid. Odor analysis of each person gives an interesting

pattern. In the morning, both volunteers have only weak armpit odor, while the odor strength increases markedly in the afternoon. It can be seen from all sensors that the left and right arms of a person yield almost equivalent signals in the morning, since no deodorant was allowed before sample collection. In contrast, the afternoon results of the left and right arms deviate distinctly. The deodorant-free left armpit expresses noticeably higher signal strength. The difference of signal strength between morning and afternoon of each armpit was tested using a paired t-test with a significance level of 95% confidence (P = 0.05). Both person A and person B have a similar pattern in the difference of signal strength between morning and afternoon. For the person A, the mean difference of left armpit and right armpit between morning and afternoon are 1.500% change of resistance (P = 0.036) and 0.700% change of resistance (P = 0.250), respectively. In case of person B, the mean difference of left armpit and right armpit between morning and afternoon are 1.365% change of resistance (P = 0.004) and 0.775% change of resistance (P = 0.054), respectively. The paired t-test shows that the signal strength of deodorant-free left armpit (P < 0.05) have statistically significant difference between morning and afternoon at the level of 95% confidence. In contrast, the changes of deodorant right armpit between morning and afternoon (P > 0.05) did not reach the level of statistical significance. In general, deodorants suppress the armpit smell by reducing bacterial activity. Hence, an interesting question arises, "can deodorant blind human identification by an E-nose ?"

To allow an identification of human odors from two persons, we have adopted a pattern analysis based on principle component analysis (PCA). Only the data from the afternoon measurement was introduced into PCA. PCA is a popular statistical technique usually used to visualize in two or three uncorrelated dimensions transformed from all correlated information. In principles, PCA process contains five following steps:

(1) Get data from matrix, $X_{M\times N}$. The row M represents different repetition of the experiment and the column N represents the number of independent sensors. In our case, M equals to 20 and N equals to 5.

(2) Normalize the data matrix, $Norm(X_{M\times N})$, by the mean subtraction. The mean of each N column is calculated and subtracted from the data set. Hence, the new data set has a zero value of mean.

(3) Calculate the covariance matrix, $Cov(X_{M\times N})$, and calculate eigenvectors and eigenvalues of the covariance matrix. The calculated eigenvectors must be unit eigenvectors.

(4) Rearrange the eigenvectors and eigenvalues. The eigenvectors are ordered by eigenvalues from highest to lowest, $(\overrightarrow{Cov(X_{M\times N})})_{\max\to\min}$.

(5) Obtain the PCA result by matrix multiplication and transpose, $\left((\overrightarrow{Cov(X_{M\times N})})_{\max\to\min} \otimes Norm(X_{M\times N})\right)^T$.

The obtained new dataset with orthogonal linear transformation are usually plotted in two or three dimensions containing the most relevant of the data set.

The PCA result is shown in Figure 7. The first principal component (PC1) explains 74.0% of the total variance and the second principal component (PC2) contributes 21.7% of the variation. The PCA result obviously distinguishes person A from person B. It indicates that each person has a specific odor pattern, even though these people have a similar life style. After both persons arrived at the laboratory, they have spent most of the time under the same humidity and temperature. The afternoon sample collection took place almost at the same time and the samples were subjected to measurement immediately. Therefore, the afternoon measurement should be more reliable than the morning one in which the odor change from bacteria could occur. The use of deodorant may not change the odor

fingerprint, though it undoubtedly reducing the strength of a key chemical such as isovaleric acid that exerts strongly on perception of body's smell. In Figure 7, each data point is plotted from day 1 to day 5. It can be seen that the odor of both armpits change everyday but PCA can still group the data of each person together. Therefore, E-nose can be a prospective candidate for identification or authentication of a person like other biometrical technologies [40].

Figure 7. The 2D-PCA of armpit odors from two persons as measured in the afternoon during 5 days.

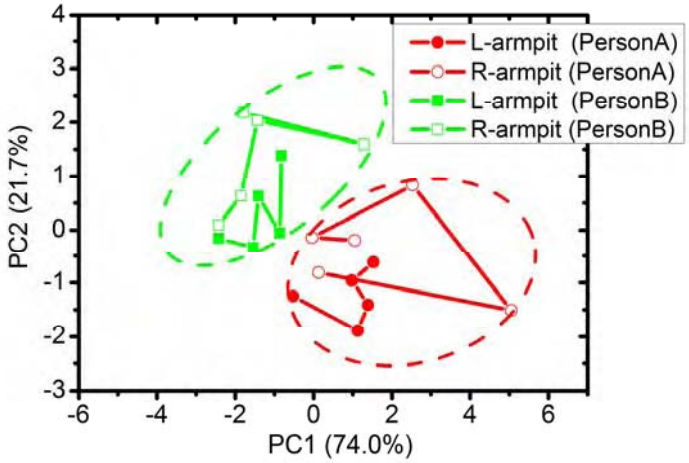

4. Conclusions

In this paper, the detection and classification of human body odor by E-nose measurement have been demonstrated. We have proposed a scheme to minimize the humidity effect that is usually a serious problem for the detection of human body odor. This scheme employs a humidity generator (hardware) for creating smooth background humidity that can dominate the humidity of samples, as well as mathematical models (software) for humidity response of all sensors that can be used to eliminate signals from the humidity in a real-time fashion. The E-nose in conjunction with PCA method was shown to differentiate the body odors of two persons with similar life style and activities. In addition, we have found that deodorant does not effect the relative identification of these two persons. In order to extend the discrimination of human body odors beyond two persons, a number of improvements are required such as increasing sensor types that response to a variety of volatile molecules. It is hoped that the preliminary results presented in this paper will open the door to the field of human body odor biometrics.

Acknowledgements

C.W. acknowledges the Commission on Higher Education for a Ph.D. scholarship under the program "Strategic Scholarships for Frontier Research Network". T.K. expresses his great gratitude to the Thailand Research Fund (BRG5180023) for a research career development grant. Mahidol University and the National Science and Technology Agency are gratefully acknowledged for supports of this research.

References and Notes

1. Barié, N.; Bücking, M.; Rapp, M. A Novel Electronic Nose Based on Miniaturized SAW Sensor Arrays Coupled with SPME Enhanced Headspace-analysis and Its Use for Rapid Determination of Volatile Organic Compounds in Food Quality Monitoring. *Sens. Actuat. B* **2006**, *114*, 482–488.
2. Vestergaard, J.S.; Martens, M.; Turkki, P. Application of an Electronic Nose System for Prediction of Sensory Quality Changes of a Meat Product (Pizza Topping) During Storage. *LWT* **2007**, *40*, 1095–1101.
3. Vinaixa, M.; Vergara, A.; Duran, C.; Llobet, E.; Badia, C.; Brezmes, J.; Vilanova, X.; Correig, X. Fast Detection of Rancidity in Potato Crisps Using E-noses Based on Mass Spectrometry or Gas Sensors. *Sens. Actuat. B* **2005**, *106*, 67–75.
4. Panigrahi, S.; Balasubramanian, S.; Gu, H.; Logue, C.M.; Marchello, M. Design and Development of a Metal Oxide Based Electronic Nose for Spoilage Classification of Beef. *Sens. Actuat. B* **2006**, *119*, 2–14.
5. Barbri, N.E.; Llobet, E.; Bari, N.E.; Correig, X.; Bouchikhi, B. Electronic Nose Based on Metal Oxide Semiconductor Sensors as an Alternative Technique for the Spoilage Classification of Red Meat. *Sensors* **2008**, *8*, 142-156.
6. Martí, M.P.; Busto, O.; Guasch, J.; Boqué, R. Electronic Noses in the Quality Control of Alcoholic Beverages. *Trends Anal. Chem.* **2005**, *24*, 57–66.
7. Yu, H.; Wang, J. Discrimination of LongJing Green-Tea Grade by Electronic Nose. *Sens. Actuat. B* **2007**, *122*, 134–140.
8. García, M.; Aleixandre, M.; Gutiérrez, J.; Horrillo, M.C. Electronic Nose for Wine Discrimination. *Sens. Actuat. B* **2006**, *113*, 911–916.
9. Dutta, R.; Hines, E.L.; Gardner, J.W.; Kashwan, K.R.; Bhuyan, M. Tea Quality Prediction Using a Tin Oxide-based Electronic Nose: an Artificial Intelligence Approach. *Sens. Actuat. B* **2003**, *94*, 228–237.
10. Scorsone, E.; Pisanelli, A.M.; Persaud, K.C. Development of an Electronic Nose for Fire Detection. *Sens. Actuat. B* **2006**, *116*, 55–61.
11. Zhang, S.; Xie, C.; Zeng, D.; Zhang, Q.; Li, H.; Bi, Z. A Feature Extraction Method and a Sampling System for Fast Recognition of Flammable Liquids with a Portable E-nose. *Sens. Actuat. B* **2007**, *124*, 437–443.
12. Zhou, H.; Homer, M.L.; Shevade, A.V.; Ryan, M.A. Nonlinear Least-Squares Based Method for Identifying and Quantifying Single and Mixed Contaminants in Air with an Electronic Nose. *Sensors* **2006**, *6*, 1–18.
13. Negri, R.M.; Reich, S. Identification of Pollutant Gases and its Concentrations with a Multisensor Array. *Sens. Actuat. B* **2001**, *75*, 172–178.
14. Chan, H.P.; Lewis, C.; Thomas, P.S. Exhaled Breath Analysis: Novel Approach for Early Detection of Lung Cancer. *Lung Cancer* **2009**, *63*, 164–168.
15. Hanson, C.W. Method and System of Diagnosing Intrapulmonary Infection Using an Electronic Nose. US Patent 6620109, 2003.
16. Pavlou, A.; Turner, A.P.F.; Barr, H. Diagnosis of Gastric and Lung Disorders, WO Patent 032091, 2000.

17. Turner, A.P.F.; Magan, N. Electronic Noses and Disease Diagnostics. *Nat. Rev. Microbiol.* **2004**, *2*, 161–166.
18. Xu, X.; Tian, F.; Yang, S.X.; Li, Q.; Yan, J.; Ma, J. A Solid Trap and Thermal Desorption System with Application to a Medical Electronic Nose. *Sensors* **2008**, *8*, 6885–6898.
19. Doty, R.L.; Ford, M.; Preti G.; Huggins, G.R. Changes in the Intensity and Pleasantness of Human Vaginal Odors during the Menstrual Cycle. *Science* **1975**, *190*, 1316–1318.
20. Chen, D.; Haviland-Jones, J. Human Olfactory Communication of Emotion. *Percept. Mot. Skills* **2000**, *91*, 771–781.
21. Delac, K.; Grgic, M. A Survey of Biometric Recognition Methods. 46th International Symposium Electronics in Marine. *ELMAR-2004*, Zadar, Croatia, June 16–18, 2004; pp. 184–193.
22. Natale, C.D.; Mantini, A.; Macagnano, A.; Antuzzi, D.; Paolesse, R.; D'Amico, A. Electronic Nose Analysis of Urine Samples Containing Blood. *Phys. Meas.* **1999**, *20*, 377–384.
23. Phillips, M.; Cataneo, R.N.; Cummin, A.R.C.; Gagliardi, A.J.; Gleeson, K.; Greenberg, J.; Maxfield, R.A.; Rom, W.N. Detection of Lung Cancer with Volatile Markers in the Breath. *Chest* **2003**, *123*, 2115–2123.
24. Phillips, M.; Cataneo, R.N.; Ditkoff, B.A.; Fisher, P.; Greenberg, J.; Gunawardena, R.; Kwon, C.S.; Rahbari-Oskoui, F.; Wong, C. Volatile Markers of Breast Cancer in the Breath. *Breast J.* **2003**, *9*, 184–191.
25. Jin, Z.; Shimbo, T.; Hosoe, Y.; Oyabu, T. Breath Odor Characteristics after Drinking and Identification of Sake Quantity. *Sens. Actuat. B* **2005**, *108*, 265–270.
26. Natale, C.D.; Macagnano, A.; Paolesse, R.; Tarizzo, E.; Mantini, A.; D'Amico, A. Human Skin Odor Analysis by Means of an Electronic Nose. *Sens. Actuat. B* **2000**, 65, 216–219.
27. Penn, D.J.; Oberzaucher, E.; Grammer, K.; Fischer, G.; Soini, H.A.; Wiesler, D.; Novotny, M.V.; Dixon, S.J.; Xu Y.; Brereton, R.G. Individual and Gender Fingerprints in Human Body Odour. *J. R. Soc. Interf.* **2007**, *4*, 331–340.
28. Pearce, T.C.; Schiffman, S.S.; Nagle, H.T.; Gardner, J.W. *Handbook of Machine Olfaction, Electronic Nose Technology*; Wiley-VCH: Weinheim, Germany, 2002.
29. Curran, A.M.; Rabin, S.I.; Prada, P.A.; Furton, K.G. Comparison of the Volatile Organic Compounds Present in Human Odor Using Spme-GC/MS. *J. Chem. Ecol.* **2005**, *31*, 1607–1619.
30. Kim, K.H.; Park, S.Y. A Comparative Analysis of Malodor Samples between Direct (Olfactometry) and Indirect (Instrumental) Methods. *Atmos. Environ.* **2008**, *42*, 5061–5070.
31. Nicell, J.A. Expressions to relate population responses to odor concentration. *Atmos. Environ.* **2003**, *37*, 4955–4964.
32. Henshaw, P.; Nicell, J.; Sikdar, A. Parameters for the Assessment of Odour Impacts on Communities. *Atmos. Environ.* **2006**, *40*, 1016–1029.
33. Akutsu, T.; Sekiguchi, K.; Ohmori, T.; Sakurada, K. Individual Comparisons of the Levels of (E)-3-Methyl-2-Hexenoic Acid, an Axillary Odor–Related Compound, in Japanese. *Chem. Senses* **2006**, *31*, 557–563.
34. Natsch, A.; Gfeller, H.; Gygax, P.; Schmid, J.; Acuna, G. A Specific Bacterial Aminoacylase Cleaves Odorant Precursors Secreted in the Human Axilla. *J. Biol. Chem.* **2003**, *278*, 5718–5727.
35. Hasegawa, Y.; Yabuki, M.; Matsukane, M. Identification of New Odoriferous Compounds in Human Axillary Sweat. *Chem. Biodiv.* **2004**, *1*, 2042–2050.

36. Hooper, D.C.; Johnson, G.A.; Peter, D. Detergent Product Containing Deodorant Compositions. US Patent 4322308, 1982.
37. Amoore, J.E. Specific Anosmia: A Clue to the Olfactory Code. *Nature* **1967**, *214*, 1095–1098.
38. Leyden, J.J.; McGinley, K.J.; Hölzle, E.; Labows, J.N.; Kligman, A.M. The Microbiology of the Human Axilla and Its Relationship to Axillary Odor. *J. Invest. Dermatol.* **1981**, *77*, 413–416.
39. Hooper, D.C.; Johnson, G.A.; Peter, D. Deodorant Compositions. US Patent 4278658, 1981.
40. Schoutena, B.; Jacobs, B. Biometrics and their Use in E-Passports. *Image Vision Comput.* **2009**, *27*, 305–312.

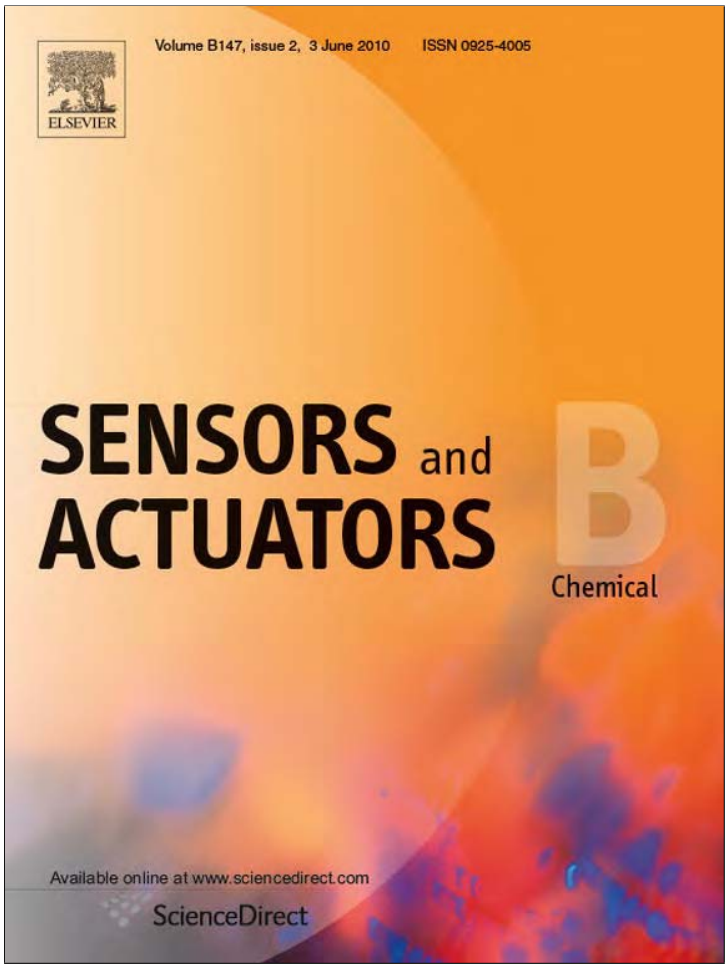

Sensors and Actuators B 147 (2010) 392–399

Contents lists available at ScienceDirect

Sensors and Actuators B: Chemical

journal homepage: www.elsevier.com/locate/snb

Portable electronic nose based on carbon nanotube-SnO_2 gas sensors and its application for detection of methanol contamination in whiskeys

Chatchawal Wongchoosuk[a], Anurat Wisitsoraat[b], Adisorn Tuantranont[b], Teerakiat Kerdcharoen[a,c,*]

[a] Department of Physics and Center of Nanoscience and Nanotechnology, Faculty of Science, Mahidol University, Bangkok 10400, Thailand
[b] Nanoelectronic and MEMS Lab, National Electronic and Computer Technology Center, Pathumthani 12120, Thailand
[c] NANOTEC Center of Excellence at Mahidol University, National Nanotechnology Center, Thailand

ARTICLE INFO

Article history:
Received 11 March 2009
Received in revised form 16 March 2010
Accepted 24 March 2010
Available online 31 March 2010

Keywords:
E-nose
Carbon nanotube
Metal oxide
Gas sensor
Feature extraction techniques

ABSTRACT

In this paper, a portable electronic nose (E-nose) based on hybrid carbon nanotube-SnO_2 gas sensors is described. The hybrid gas sensors were fabricated using electron beam (E-beam) evaporation by means of powder mixing. The instrument employs feature extraction techniques including integral and primary derivative, which lead to higher classification performance as compared to the classical features (ΔR and $\Delta R/R_0$). It was shown that doping of carbon nanotube (CNT) improves the sensitivity of hybrid gas sensors, while quantity of CNT has a direct effect on the selectivity to volatile organic compounds, i.e., methanol (MeOH) and ethanol (EtOH). The real-world applications of this E-nose were also demonstrated. Based on the proposed methods, this instrument can monitor and classify 1 vol% of MeOH contamination in whiskeys.

1. Introduction

Nowadays, electronic nose (E-nose) has become a powerful tool to evaluate the aroma compounds during the quality control process of foods and beverages [1–3]. Besides, E-noses have also been employed for public safety [4], environment protection [5,6], disease diagnostics [7], etc. E-nose is composed of an array of gas sensors made from various materials that display distinct gas-sensing behaviors of which differentiation can be combined and interpreted via pattern recognition techniques [8]. Among the available sensing materials, metal oxide semiconductors (MOS), such as SnO_2 and WO_3, have been the most popular due to their high sensitivity to a rich set of volatile compounds.

Doping has long been used as a traditional mean to obtain new MOS gas sensors that exhibit gas-sensing properties differentiated from the original ones. Recently, much interest has been focused on carbon nanotube (CNT) as potential dopant, due to its special electronic properties and high specific surface area that can boost catalytic reactions occurring at the metal oxide surface. The hybrid CNT–SnO_2 gas sensors prepared by different techniques have been reported to have excellent responses to NO_2 [9,10], CO [10], NH_3 [11], H_2 [12], CHOH [13] and indoor air pollutants [14]. Among such techniques, co-evaporation of SnO_2/CNT is a relatively new concept to form hybrid CNT–SnO_2 gas sensors [15,16]. It offers extensive possibilities for controlling the film structure and morphology with high deposition rates, low contamination, high reliability and high productivity. However, there have been very few reports on CNT–SnO_2 gas sensors prepared by this technique, and this sensor system has not been applied for E-nose applications.

In this work, we report on an E-nose based on hybridized CNT–SnO_2 gas sensors prepared by electron beam (E-beam) evaporation, which is inexpensive, fast, portable, reliable and suitable for use for the detection and classification of both solid and liquid samples. In addition, feature extraction techniques including integral and primary derivative are proposed for improving classification performance by principal component analysis (PCA). This E-nose was tested in a real-world application, i.e., for detecting methanol (MeOH) contaminant in whiskeys. This system will be a useful tool for quality assurance of whiskey produced by village industries.

2. Experimental

2.1. Fabrication of gas sensors

The gas sensors were fabricated by E-beam evaporation. Top and cross-sectional views of sensor structure are shown in Fig. 1a and b, respectively. First, Cr/Au interdigitated electrodes on alumina substrates were prepared. Prior to deposition of the electrodes,

* Corresponding author at: Department of Physics and Center of Nanoscience and Nanotechnology, Faculty of Science, Mahidol University, Bangkok 10400, Thailand. Tel.: +66 866037395; fax: +66 22015843.
E-mail address: sctkc@mahidol.ac.th (T. Kerdcharoen).

0925-4005/$ – see front matter © 2010 Elsevier B.V. All rights reserved.
doi:10.1016/j.snb.2010.03.072

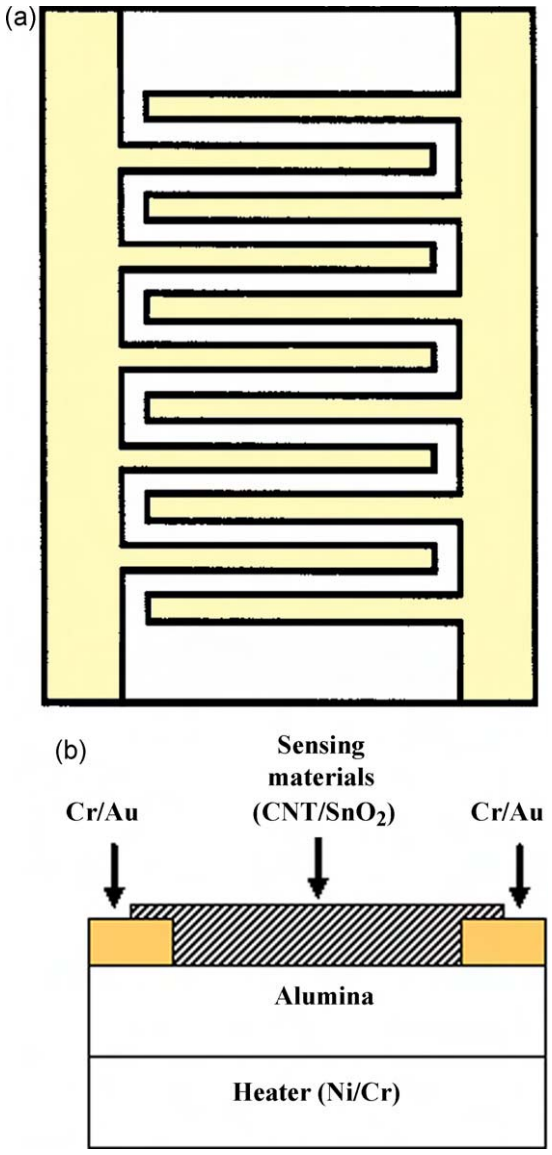

Fig. 1. Structure of the gas sensor; (a) top view of interdigitated electrode, (b) cross-sectional view.

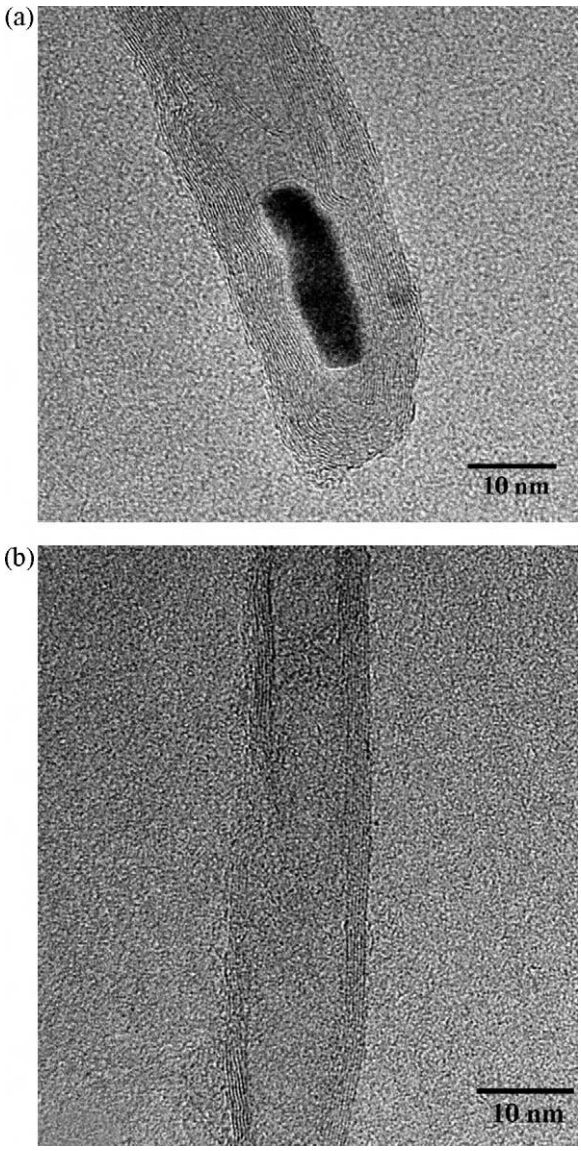

Fig. 2. Typical TEM images of multi-walled CNT (a) before and (b) after purification.

the substrates were cleaned by oxygen-ion bombardment under a vacuum pressure of $\sim 10^{-4}$ Torr in order to improve the adhesion of the film to the substrates. Cr and Au layers were then successively E-beam evaporated over the alumina substrates through electroplated-Ni shadow masks. These shadow masks were fabricated by means of standard photolithography and electroplating of Ni. The masks were employed by attaching them to the substrates using strong magnets. The resulted thickness of Cr and Au layers were ~50 nm and ~200 nm, respectively. The width, spacing, and length of the interdigitated electrodes are approximately 100 μm, 100 μm, and 1 mm, respectively.

Multi-walled CNT powder was synthesized by thermal chemical vapor deposition (CVD) in a lab-made horizontal tube furnace. Iron catalyst powder was loaded in the tube furnace and heated up until the growth temperature of 700 °C was reached. The system was then maintained under the hydrogen gas flow of 1.5 l/min at the atmospheric pressure. Next, acetylene gas was introduced into the system for 2 h for CNT synthesis. The flow ratio between acetylene and hydrogen was approximately 1:4. The remaining catalysts were removed from CNTs by chemical oxidation in 4 M nitric acid at room temperature for 4 h. Then, CNTs were rinsed with DI water and dehydrated at 150 °C for 2 h [17]. Transmission electron microscope (TEM) images of the CNT before and after chemical oxidation treatments are shown in Fig. 2a and b, respectively. It is evident that the iron catalysts were effectively removed and the number of CNT walls was reduced.CNT–SnO_2 mixed powders were prepared with 0.5 wt% and 1 wt% concentrations by mixing 15 g of SnO_2 powder with 0.075 g and 0.15 g of CNT powders, respectively. The mixed powders were thoroughly mixed by grinding in a mortar for 30 min. The pure SnO_2 and mixed powders were compressed into cylindrical pellets in a hard steel mold by a hydraulic compressor at a pressure of 15 tons. Next, the compressed SnO_2 and mixed CNT–SnO_2 materials (0.5 wt% and 1 wt% CNTs) were loaded in E-beam chamber and evaporated over the interdigitated electrodes through an electroplated shadow mask with square window pattern that aligned to the interdigitated area at an operating vacuum of $\sim 10^{-5}$ Torr. The evaporation condition was based on the previous studies by Wisitsoraat et al. [15,16]. The film thickness of sensing materials is ~300 nm as measured *in situ* by quartz crystal monitor. The evaporated film was then annealed at 500 °C for 3 h. Finally, a NiCr (Ni 80% and Cr 20%) layer was also E-beam evaporated over the backside of substrate to perform as a heating unit. The NiCr heater

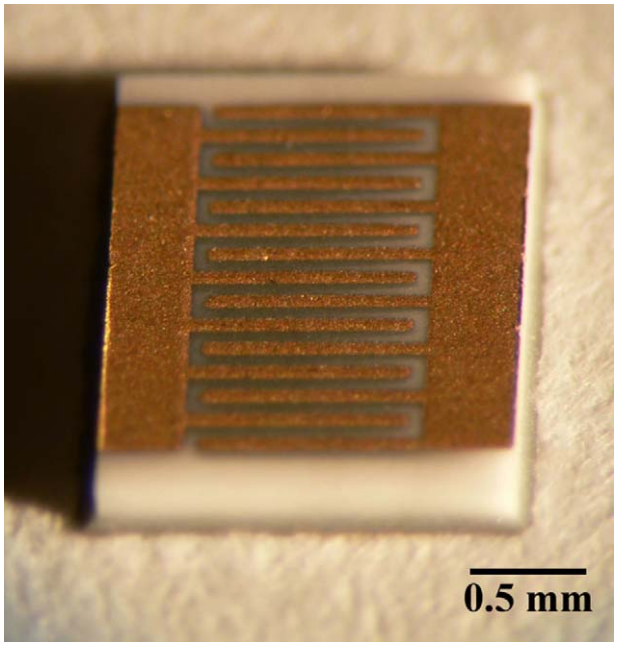

Fig. 3. Photograph of the fabricated sensor.

can perform heating up to 350 °C. A photograph of fabricated sensor is shown in Fig. 3.

2.2. Portable E-nose system

An E-nose has been developed in a briefcase form factor (19.5 cm × 29.5 cm × 10 cm). Fig. 4 shows a schematic diagram indicating the key components of the portable E-nose system. The clean air produced from a pump carries aroma molecules of sample into a sensor chamber at flow rate 2 l/min. Four electrical solenoid valves were used to avoid mixing of gas from the reference and the sample. It is necessary for this type of measurement to switch between a reference and a sample glass in order to reduce the humidity effects [18,19].

The sensor array consisting of three gas sensors: SnO_2, 0.5 wt% CNT–SnO_2 and 1 wt% CNT–SnO_2 was symmetrically embedded at the bottom of a Teflon chamber. A simple linear circuit, called as voltage divider, was employed for measuring the resistance of each gas sensor. The load resistance is 20 kΩ ± 1% while the resistance of each gas sensor lies within the range 20–40 kΩ. The voltage input is fixed at 5 V. The data were collected every second by a notebook computer using a data acquisition card (NI-DAQ 6008) under LabVIEW software for subsequent analyses.

2.3. PCA and feature extraction techniques

PCA was used for pattern recognition and classification of samples measured by the portable E-nose. PCA is a statistical technique that allows an easy visualization of all correlated information [20]. In principles, PCA process contains five steps as follows:

i. Get data from matrix, $X_{M\times N}$. The row M represents different repetition of the experiment and the column N represents the number of independent sensors.
ii. Normalize the data matrix, $Norm(X_{M\times N})$, by the mean subtraction. The mean of each N column is calculated and subtracted from the data set. Hence, the new data set produces the mean equal to zero.
iii. Calculate the covariance matrix, $Cov(X_{M\times N})$, and calculate eigenvectors and eigenvalues of the covariance matrix. The calculated eigenvectors must be unit eigenvectors.
iv. Rearrange the eigenvectors and eigenvalues. The eigenvectors are ordered by eigenvalues from highest to lowest, $(\overrightarrow{Cov(X_{M\times N})})_{\max\rightarrow\min}$.

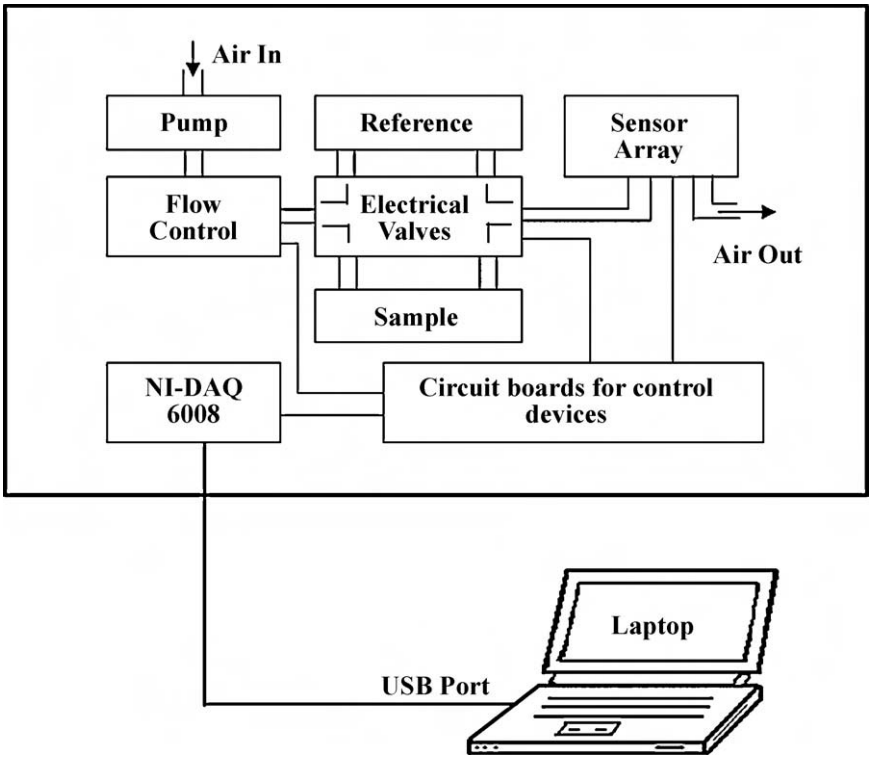

Fig. 4. Schematic diagram of the portable E-nose system.

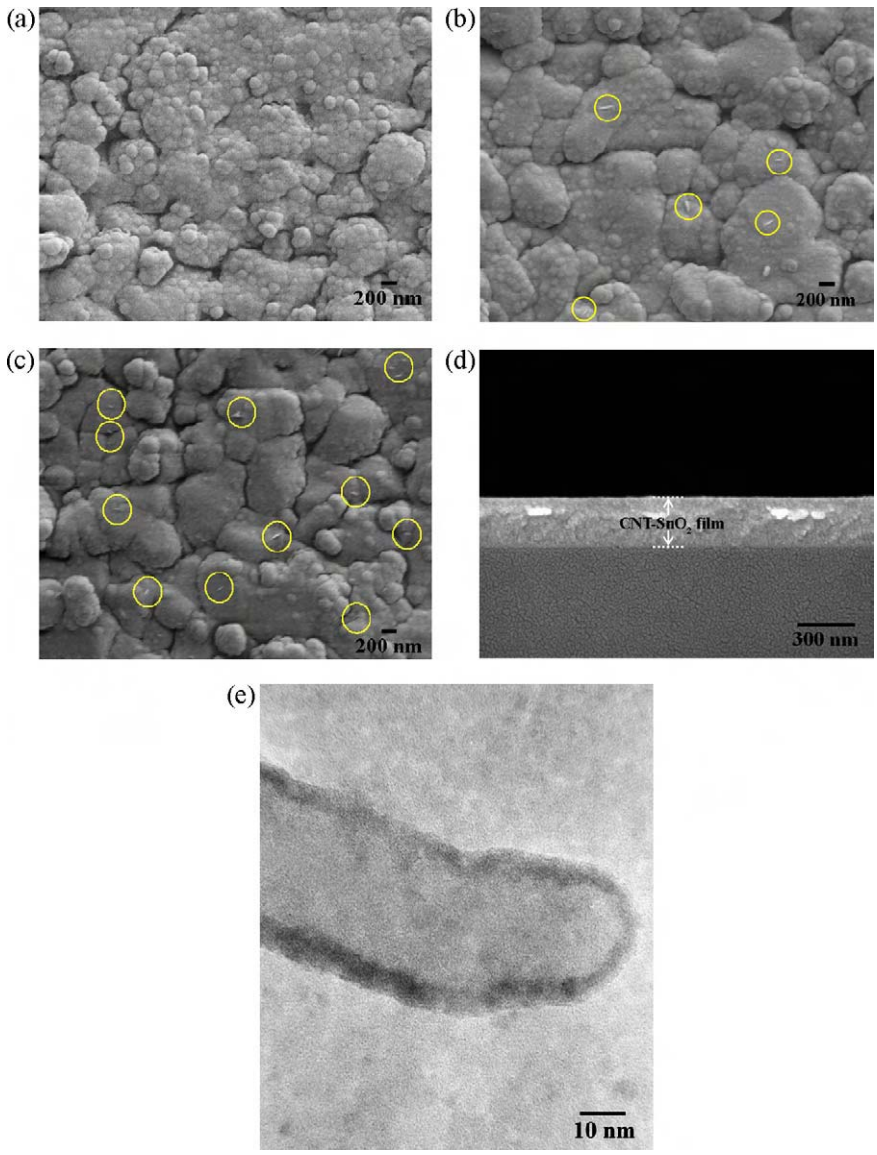

Fig. 5. SEM images of sensing films; (a) undoped SnO_2 film, (b) 0.5 wt% CNT–SnO_2 film and (c) 1 wt% CNT–SnO_2 film. The yellow circles in (b) and (c) indicate CNT fragments, (d) typical cross-sectional SEM image of CNT–SnO_2 film and (e) typical HRTEM image of CNT–SnO_2 film.

v. Obtain the PCA result by matrix multiplication and transpose, $\left((\overrightarrow{Cov(X_{M\times N})})_{\max\to\min} \otimes Norm(X_{M\times N})\right)^T$. The obtained new data set with orthogonal linear transformation has been plotted in two or three dimensions containing the most relevant of the data set.

However, preprocessing or feature extraction from the acquired sensor signal prior to the use of PCA is very necessary to get better separation. Two features: integral and primary derivative, having specific physical meanings were proposed as the following formulation:

$$\text{Integral}: \quad I_t = \int_a^b V_{out}\,dt \tag{1}$$

$$\text{Primary derivative}: \quad D_t = \frac{dV_{out}}{dt} \tag{2}$$

where V_{out} represents a sensor signal.

In real calculation, the integral and primary derivative of V_{out} are obtained from the elements of y_i^I and y_i^D, respectively, using the following relations:

$$y_i^I = \frac{1}{6}\sum_{j=0}^{i}(x_{j-1} + 4x_j + x_{j+1})dt \tag{3}$$

$$y_i^D = \frac{1}{2dt}(x_{i+1} - x_{i-1}) \tag{4}$$

where $i = 0, 1, 2, \ldots, n-1$ and n is the number of samples.

In addition, signal integral refers to the accumulative total of the reaction degree-changing while primary derivative of signal represents the reaction rate [21,22].

3. Results and discussion

3.1. Characterization of gas-sensing films

Fig. 5a–c illustrates morphology of the sensing films by scanning electron microscopy (SEM), showing the presence of metal oxide grains. Spherical SnO_2 particles are clearly observed in the undoped tin oxide film (see Fig. 5a). In the CNT-doped SnO_2 films, such spherical particles are smoothed out and smaller SnO_2 grain

sizes are observed. In addition, the CNTs are well embedded and randomly arranged inside the SnO_2 film as circled in Fig. 5b and c. It can be seen that although the distributions of CNTs in the films are quite random, the densities of the observed CNTs are proportional to the concentration of CNTs in the initial mixed powders. Therefore, the amount of CNTs in the film can be well controlled by varying the percentage of CNTs in the initial mixed powder.

Typical cross-sectional SEM image of CNT-doped SnO_2 film is shown in Fig. 5d. It indicates that the film thickness is about 270 nm, slightly lower than the expected value of 300 nm. The small discrepancy should be due to some calibration inaccuracies of quartz crystal monitor. The detailed structure of CNT–SnO_2 composite was characterized by high-resolution TEM (HRTEM). The samples were prepared by E-beam evaporation of SnO_2/CNT onto carbon coated copper TEM grid, which was done at the same time as coating on interdigitated electrodes. A typical HRTEM image of CNT–SnO_2 composite is shown in Fig. 5e. From the HRTEM image, it can be identified that a single multi-walled CNT fragment is indeed embedded in the nanocrystalline SnO_2 layer. The diameter of CNTs and the crystal size of SnO_2 were estimated to be in the range of ~20–40 nm and 3–10 nm, respectively. Comparing to the TEM image of pure CNT (Fig. 2b), the nanotube walls cannot be resolved due to the presence of SnO_2 nanocrystalline thin film surrounding the surface of CNT.

A plausible mechanism for CNT–SnO_2 co-evaporation can be drawn as follows. When SnO_2 was evaporated at temperature of ~1500 °C in a vacuum of ~10^{-5} Torr, CNTs fragments, which are small and very light, were carried into the vapor by surrounding SnO_2 molecules. It should be noted that CNTs themselves were not decomposed during evaporation because this temperature is well below CNTs' sublimation point (>3000 °C) in a high vacuum condition. Thus, these results prove our new concept that CNTs can be co-evaporated with SnO_2 material with no significant decomposition at the evaporation temperature of ~1500 °C. In addition, CNTs can endure treatment of high-energy electron beams (~7.67 kV) in a high vacuum of 10^{-5} Torr. When CNT molecular fragments arrived at the substrate that was held at 130 °C, SnO_2 vapor was condensed and coated around them. As the substrate was cooled down, CNTs remained in the lattice of SnO_2 due to physicochemical binding between SnO_2 and CNTs. This result is evident as seen in the TEM and SEM images. The fact that there should be physical binding between SnO_2 and CNTs can also be inferred from other reports that demonstrate SnO_2 coating around CNTs [9–14].

3.2. Sensor responses

The produced sensors were placed in a desiccator that served as a gas sensitivity test chamber. The total volume of the chamber is 22.35 l. Gas response (S) is calculated as follows:

$$S = \frac{R_{gas}}{R_{air}} \quad (5)$$

where R_{air} and R_{gas} are the resistances of the sensor in air and in the presence of desired gas, respectively.

The undoped SnO_2 sensor, 0.5 wt% CNT–SnO_2 sensor and 1 wt% CNT–SnO_2 sensor show response to ethanol (EtOH) and methanol

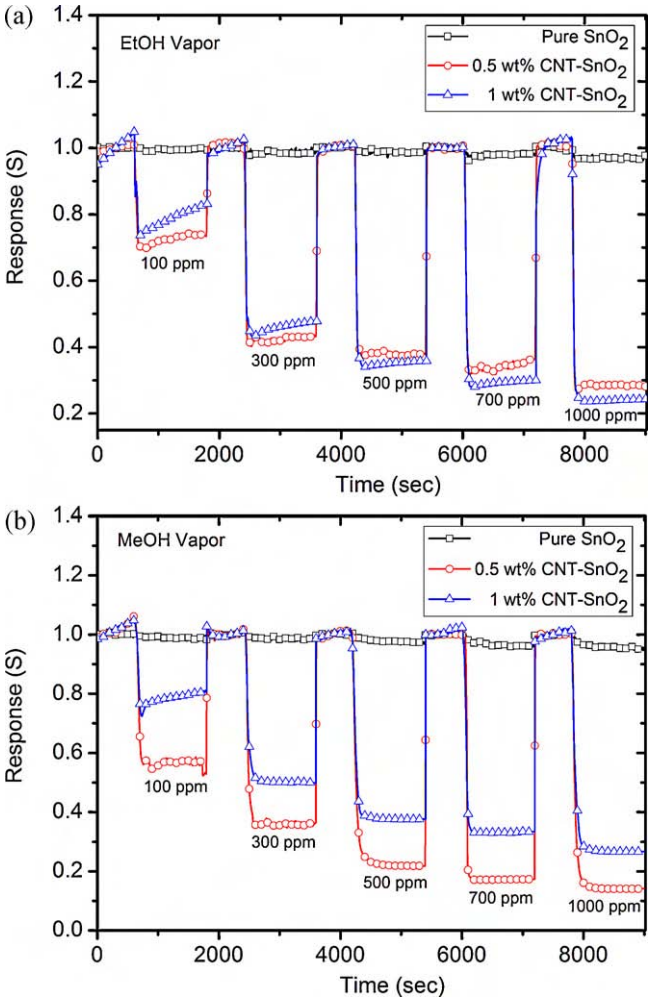

Fig. 6. Sensor responses of undoped SnO_2 sensor, 0.5 wt% CNT–SnO_2 sensor and 1 wt% CNT–SnO_2 sensor to different concentrations of (a) EtOH and (b) MeOH.

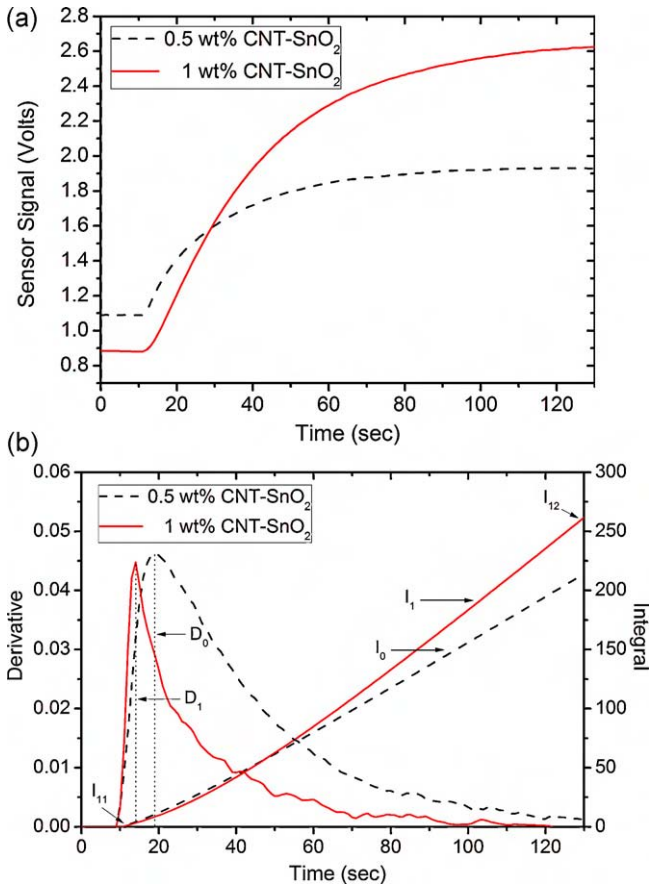

Fig. 7. (a) Raw responses (b) primary derivative and integral signals of gas sensors measured using portable E-nose.

(MeOH) as shown in Fig. 6a and b, respectively. It should be noted that the selected film thickness of 300 nm is an optimized value for electrical conductivity and sensitivity. It was found from our study that sensors with thickness of less than 200 nm and more than 400 nm will have too low and too high electrical conductivity, respectively. In addition, the gas-sensing response is increased as thickness increases from 50 nm to 200 nm and the response becomes quite independent of thickness as the thickness increases from 200 nm to 400 nm and begins to slowly decrease as the thickness increases further. In addition, a variation of less than 30% was found among ten tested sensors and the sensors have a long term drift of less than 20% over 6 months of operation. Thus, the fabricated sensors have reasonably good reproducibility and stability.

From Fig. 6, it can be seen that these materials behave as n-type semiconductors since their resistance decreases in the presence of a deoxidizing gas, whereas MWCNT–SnO_2 film prepared by spin-coating technique behave as p-type semiconductors [11]. Under the operating temperature range ~250–300 °C, CNT doping can improve the response of gas sensor on EtOH and MeOH compared with the pure SnO_2 sensor. The response of native SnO_2 sensor is lower than 2% while CNT-doped SnO_2 sensors give the response higher than 65% at concentration 1000 ppm under such temperature range. The amount of CNT doping exhibits different change in response to EtOH and MeOH vapors. Hence, the 0.5 wt% and 1 wt% of CNTs show highest response toward MeOH and EtOH, respectively. These results confirm that varying of CNT concentration can be used to tune sensitivity and selectivity of SnO_2 sensor to a desired gas. In this case, the modified gas sensors can be employed to target MeOH vapor in the MeOH/EtOH mixture. Nevertheless, if CNT amount exceed, the gas sensitivity will be reduced because the CNTs begin to connect together and result in shorter resistance path [15].

3.3. Sensing mechanism of CNT–SnO_2 gas sensors

From the gas-sensing data, small percentage of CNT doping significantly enhances the sensing of MeOH and EtOH. The results are consistent with other reports based on CNT–SnO_2 composites [9–15]. In these reports, various explanations for gas-sensing enhancement by CNTs have been proposed, for examples, amplification effect of the PN junction structure between n-SnO_2 and p-SWCNT [9], the oriented growth of SnO_2 along the CNTs during heat treatment and its consequent enhancement of the local electric field favorable for the gas-sensing reaction [14] and increased surface area due to the formation of CNT protrusions [15]. The PN junction structure between SnO_2 and SWCNT is not applied in the present case because MWCNTs are used.

In this work, we propose that the observed enhancement effect is attributed to the nanochannels formed by MWCNTs embedded in SnO_2. The formation of the nanochannels in SnO_2 surface can increase the diffusion of the gas molecules into the metal oxide surface as well as enhance local electric field at CNT–SnO_2 interface. This can considerably enhance dehydrogenation reactions of MeOH

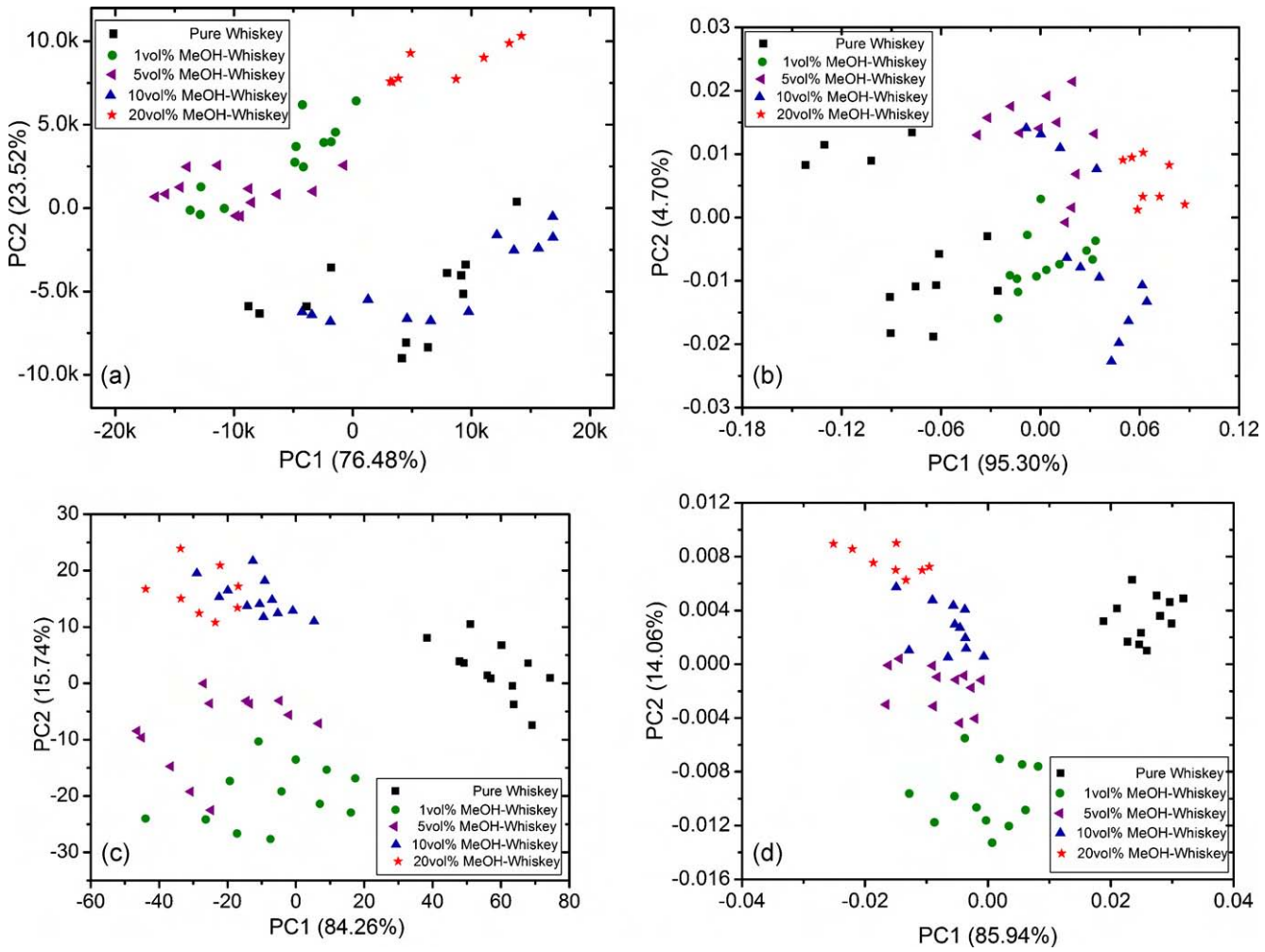

Fig. 8. PCA results using feature extraction from (a) ΔR, (b) $\Delta R/R_0$ and (c) integral and (d) primary derivative.

and EtOH as described by [23]:

$$2CH_3OH + O_2 \rightarrow 2CH_3O + H_2O + e^- \quad (6)$$

$$2CH_3CH_2OH + O_2 \rightarrow 2CH_3CHO + H_2O + e^- \quad (7)$$

Since the effect of CNTs on gas sensing is primarily on the surface, the gas-sensing response is not significantly dependent on the thickness when the thickness is sufficiently large. This is in accordance with our observations. Increasing surface area due to CNTs intrusion and observed smaller grain size due to CNTs doping can partly contribute to enhancing gas reaction. However, the contribution from these effects is relatively small because CNT concentration is so low that the specific surface area is only slightly affected by CNTs inclusion.

3.4. Electronic nose with PCA analysis

Since the fabricated sensors show different response to EtOH and MeOH, the E-nose based on such sensors can be applied to monitor MeOH contaminant in whiskey. Typical E-nose response to a whiskey is displayed in Fig. 7a while the integral and primary derivative of the response are shown in Fig. 7b. Because pure SnO_2 sensor gives a tiny response, the signal obtained from the pure SnO_2 sensor was neglected in further analysis.

From each sensor response curve, four different features were extracted for each sample. The first feature extraction is the conductance change, defined as $\Delta R = R_{gas} - R_0$. The second feature extraction is the relative response ($\Delta R/R_0$). The third feature extraction is the integral. This feature was extracted by calculation of difference accumulative total reaction in the presence of sample gas, i.e., $I_{12} - I_{11}$ (see Fig. 7b). The last one is the primary derivative. The maximum amplitude in the same interval was employed, i.e., D_0 and D_1 (see Fig. 7b). Each data set extracted from each proposed feature in the form of $X_{56\times2}$ is introduced into the PCA process. PCA results of the data sets extracted by the proposed methods; ΔR, $\Delta R/R_0$, integral and primary derivative are shown in Fig. 8a–d, respectively.

The PCA results show that the feature extraction based on ΔR cannot classify the contamination of MeOH in whiskey due to the drift effect of sensor signal depending on temperature variation in the long time measurement. The classical relative response ($\Delta R/R_0$) seems to give a better result than ΔR but many samples disperse in the same region and pure whiskey results locate rather close to whiskey having 1 vol% of MeOH contamination while MeOH content exceeding 2% (v/v) would harm the consumer [24]. In such case, the resolution power is not enough to guarantee the contamination of MeOH in whiskey. For feature extraction using both the integral and primary derivative data treatments, PCA results show a perfect classification between pure whiskey and whiskey having MeOH contamination. Moreover, the primary derivative can cluster all level of MeOH contaminations (1 vol%, 5 vol%, 10 vol% and 20 vol%) in the whiskey as shown in Fig. 8d. These results indicate that the proposed feature extractions, integral and primary derivative, provide good capabilities in the recognition and discrimination of MeOH contamination. These may be alternative ways to replace the common methods (ΔR and $\Delta R/R_0$) which are widely used in PCA analysis.

From our PCA results together with feature extraction technique, it can be seen that although the sensors are structurally similar, they can have sufficiently distinct response such that it can be used to discriminate different kind of similar odors. However, it should be noted that features extracted from response behaviors can be dependent on some measuring details such as chamber size, gas flow rate, and sensor position in the sensor chamber. Consequently, the feature extraction result can be considerably different for different E-nose systems. Nevertheless, it should not be a problem for E-nose applications because this can be well controlled for each E-nose system and any E-nose system must always be trained under a fixed condition.

4. Conclusions

We have reported the design, implementation and an example application of portable E-nose based on CNT–SnO_2 gas sensors including new feature extraction methods for improvement of data classification. The doping of CNTs could enhance the sensitivity of SnO_2 sensor while their concentration plays an important role in selectivity to volatile organic compounds such as EtOH and MeOH. The PCA results indicate that the newly proposed feature extraction including integral and primary derivative leads to higher classification performance as compared to the standard features (ΔR and $\Delta R/R_0$). The portable E-nose based on only two nanostructure sensors combined with proposed feature extraction methods shows clearly the classification of MeOH contamination mixed in the whiskey at higher concentrations than 1% by volume. It is hoped that such E-nose will be a useful tool for the whiskey industry and for quick screening of village-made whiskeys that are usually found of the MeOH contaminant.

Acknowledgements

C.W. acknowledges the Commission on Higher Education for a Ph.D. scholarship under the program “Strategic Scholarships for Frontier Research Network”. T.K. expresses his great gratitude to the Thailand Research Fund (BRG5180023) for a research career development grant. Mahidol University and the National Science and Technology Agency are gratefully acknowledged for supports.

References

[1] M.P. Marti, R. Boque, O. Busto, J. Guasch, Electronic noses in the quality control of alcoholic beverages, Trends Anal. Chem. 24 (2005) 57–66.
[2] H. Yu, J. Wang, Discrimination of Long Jing green-tea grade by electronic nose, Sens. Actuators B, Chem. 122 (2007) 134–140.
[3] J.S. Vestergaard, M. Martens, P. Turkki, Application of an electronic nose system for prediction of sensory quality changes of a meat product (pizza topping) during storage, LWT 40 (2007) 1095–1101.
[4] E. Scorsone, A.M. Pisanelli, K.C. Persaud, Development of an electronic nose for fire detection, Sens. Actuators B, Chem. 116 (2006) 55–61.
[5] R.M. Negri, S. Reich, Identification of pollutant gases and its concentrations with a multisensor array, Sens. Actuators B, Chem. 75 (2001) 172–178.
[6] A.C. Bastos, N. Magan, Soil volatile fingerprints: use for discrimination between soil types under different environmental conditions, Sens. Actuators B, Chem. 125 (2007) 556–562.
[7] A.P.F. Turner, N. Magan, Electronic noses and disease diagnostics, Nat. Rev. Microbiol. 2 (2004) 161–166.
[8] M. Pardo, G. Sberveglieri, Comparing the performance of different features in sensor arrays, Sens. Actuators B, Chem. 123 (2007) 437–443.
[9] B.Y. Wei, M.C. Hsu, P.G. Su, H.M. Lin, R.J. Wu, H.J. Lai, A novel SnO_2 gas sensor doped with carbon nanotubes operating at room temperature, Sens. Actuators B, Chem. 101 (2004) 81–89.
[10] E.H. Espinosa, R. Ionescu, B. Chambon, G. Bedis, E. Sotter, C. Bittencourt, A. Felten, J.J. Pireaux, X. Correig, E. Llobet, Hybrid metal oxide and multiwall carbon nanotube films for low temperature gas sensing, Sens. Actuators B, Chem. 127 (2007) 137–142.
[11] N.V. Hieu, L.T.B. Thuya, N.D. Chien, Highly sensitive thin film NH_3 gas sensor operating at room temperature based on SnO_2/MWCNTs composite, Sens. Actuators B, Chem. 129 (2008) 888–895.
[12] J. Gong, J. Sun, Q. Chen, Micromachined sol–gel carbon nanotube/SnO_2 nanocomposite hydrogen sensor, Sens. Actuators B, Chem. 130 (2008) 829–835.
[13] J. Wang, L. Liu, S.Y. Cong, J.Q. Qi, B.K. Xu, An enrichment method to detect low concentration formaldehyde, Sens. Actuators B, Chem. 134 (2008) 1010–1015.
[14] J. Liu, Z. Guo, F. Meng, Y. Jia, J. Liu, A novel antimony-carbon nanotube-tin oxide thin film: carbon nanotubes as growth guider and energy buffer. Application for indoor air pollutants gas sensor, J. Phys. Chem. C 112 (2008) 6119–6125.
[15] A. Wisitsoraat, A. Tuantranont, C. Thanachayanont, V. Patthanasettakul, P. Singjai, Electron beam evaporated carbon nanotube dispersed SnO_2 thin film gas sensor, J. Electroceram. 17 (2006) 45–49.
[16] A. Wisitsoraat, A. Tuantranont, V. Patthanasettakul, T. Lomas, P. Chindaudom, Ion-assisted e-beam evaporated gas sensor for environmental monitoring, Sci. Technol. Adv. Mater. 6 (2005) 261–265.

[17] H. Liu, G. Cheng, R. Zheng, Y. Zhao, C. Liang, Influence of synthesis process on preparation and properties of Ni/CNT catalyst, Diamond Relat. Mater. 15 (2006) 15–21.
[18] T.C. Pearce, S.S. Schiffman, H.T. Nagle, J.W. Gardner, Handbook of Machine Olfaction; Electronic Nose Technology, Wiley-VCH, 2002.
[19] C. Wongchoosuk, M. Lutz, T. Kerdcharoen, Correction of humidity effect for detection of human body odor, in: Proceedings of the 5th ECTI-CON 2, 2008, pp. 845–848.
[20] I.T. Jolliffe, Principal Component Analysis, Springer, 2002.
[21] S. Roussel, G. Forsberg, V. Steinmetz, P. Grenier, V. Bellon-Maurel, Optimisation of electronic nose measurement. Part I. Methodology of output feature selection, J. Food Eng. 37 (1998) 207–222.
[22] S. Zhang, C. Xie, D. Zeng, Q. Zhang, H. Li, Z. Bi, A feature extraction method and a sampling system for fast recognition of flammable liquids with a portable E-nose, Sens. Actuators B, Chem. 124 (2007) 437–443.
[23] S. Majumder, S. Hussain, S.N. Das, R.B. Bhar, A.K. Pal, Silicon doped SnO_2 films for liquid petroleum gas sensor, Vacuum 82 (2008) 760–770.
[24] A.J. Paine, A.D. Dayan, Defining a tolerable concentration of methanol in alcoholic drinks, Hum. Exp. Toxicol. 20 (2001) 563–568.

Biographies

Chatchawal Wongchoosuk received his B.Sc. with first class honors from Prince of Songkla University in 2005 and M.Sc. from Mahidol University in 2007 on Physics. At present, he is a Ph.D. student at the Department of Physics, Mahidol University. His current research interests involve electronic noses, hybrid gas sensors and molecular simulation.

Anurat Wisitsoraat received his Ph.D., M.S. degrees from Vanderbilt University, TN, U.S.A., and B.Eng. degree in Electrical Engineering from Chulalongkorn University, Bangkok, Thailand in 2002, 1997, and 1993, respectively. His research interests include microelectronic fabrication, semiconductor devices, electronic and optical thin film coating, gas sensors, and micro-electromechanical systems (MEMS).

Adisorn Tuantranont is currently Lab director of Nanoelectronics and MEMS Laboratory, National Electronics and Computer Technology Center (NECTEC), under National Science and Technology Development Agency (NSTDA), Thailand. He received the B.S. degree from King Mongkut's Institute of Technology Ladkrabang (KMITL), Bangkok, Thailand in 1995, and the Ph.D. degree in 2001 from University of Colorado at Boulder, CO, USA, in Electrical Engineering. His current research interests are optical MEMS, microfluidic lab-on-a-chip and optoelectronics packaging.

Teerakiat Kerdcharoen received B.Sc. and M.Sc. in Chemistry from Chulalongkorn University in 1990 and 1992, respectively. As an Exchange Student, he received his Ph.D. in Physical Chemistry from University of Innsbruck in 1995. Presently, he is a faculty member of Mahidol University. His research interests cover the topics of organic electronics ranging from theoretical modeling of materials to fabrication of devices such as tactile and chemical sensors.

Sensors **2010**, *10*, 7705-7715; doi:10.3390/s100807705

OPEN ACCESS

sensors

ISSN 1424-8220

www.mdpi.com/journal/sensors

Article

Multi-Walled Carbon Nanotube-Doped Tungsten Oxide Thin Films for Hydrogen Gas Sensing

Chatchawal Wongchoosuk [1], Anurat Wisitsoraat [2], Ditsayut Phokharatkul [2], Adisorn Tuantranont [2] and Teerakiat Kerdcharoen [1,3,*]

[1] Department of Physics and Center of Nanoscience and Nanotechnology, Faculty of Science, Mahidol University, Ratchathewee, Bangkok 10400, Thailand; E-Mail: g5037004@student.mahidol.ac.th

[2] Nanoelectronics and MEMS Laboratory, National Electronics and Computer Technology Center, Klong Luang, Pathumthani 12120, Thailand; E-Mails: anurat.wisitsoraat@nectec.or.th (A.W.); ditsayut.phokharatkul@nectec.or.th (D.P.); adisorn.tuantranont@nectec.or.th (A.T.)

[3] NANOTEC Center of Excellence at Mahidol University, National Nanotechnology Center, Thailand

* Author to whom correspondence should be addressed; E-Mail: sctkc@mahidol.ac.th; Tel.: +6-622-015-770; Fax: +6-622-015-843.

Received: 20 June 2010; in revised form: 15 July 2010 / Accepted: 30 July 2010 / Published: 17 August 2010

Abstract: In this work we have fabricated hydrogen gas sensors based on undoped and 1 wt% multi-walled carbon nanotube (MWCNT)-doped tungsten oxide (WO_3) thin films by means of the powder mixing and electron beam (E-beam) evaporation technique. Hydrogen sensing properties of the thin films have been investigated at different operating temperatures and gas concentrations ranging from 100 ppm to 50,000 ppm. The results indicate that the MWCNT-doped WO_3 thin film exhibits high sensitivity and selectivity to hydrogen. Thus, MWCNT doping based on E-beam co-evaporation was shown to be an effective means of preparing hydrogen gas sensors with enhanced sensing and reduced operating temperatures. Creation of nanochannels and formation of p-n heterojunctions were proposed as the sensing mechanism underlying the enhanced hydrogen sensitivity of this hybridized gas sensor. To our best knowledge, this is the first report on a MWCNT-doped WO_3 hydrogen sensor prepared by the E-beam method.

Keywords: WO_3; hydrogen sensor; nanochannels; E-beam evaporation; carbon nanotube

1. Introduction

Hydrogen (H_2) is one of the most useful gases, being used in many chemical processes and various industries including aerospace, medical, petrochemical, transportation, and energy [1-3]. In recent years, H_2 has attracted a great deal of attention as a potential clean energy source for the next generation of automobiles and household appliances due to its perfectly clean combustion without any release of pollutants or greenhouse gases [4]. However, this low molecular weighted gas can easily leak out and may cause fires or explosions when its concentration in air is between 4% and 75% by volume [5]. Moreover, H_2 is a colorless, odorless and tasteless gas that cannot be detected by human senses. Therefore, it is very essential to develop the effective H_2 gas sensors for monitoring of H_2 leaks.

Tungsten Oxide (WO_3) is one of the most widely studied gas-sensing materials due to its fast, high sensitivity response toward NO_x [6-9], H_2S [10-13], C_2H_5OH [13,14] CO [15], NH_3 [15-19] and O_3 [20]. In case of H_2 detection, it is well known that H_2 molecules are not activated on the smooth WO_3 surface of single crystals [21]. Addition of some noble metals such as Pt, Pd, or Au [22-26] to WO_3 usually improves the sensitivity and selectivity to H_2 gas. These metal doped WO_3 films can be prepared by several methods, including screen printing [22], sputtering [23,24] and sol-gel process [25,26].

In the present work, multi-walled carbon nanotube (MWCNT)-doped WO_3 thin films fabricated by an electron beam (E-beam) evaporation process and their application for H_2 gas sensing are reported for the first time. The E-beam process offers extensive possibilities for controlling film structure and morphology with desired properties such as dense coating, high thermal efficiency, low contamination, high reliability and high productivity. MWCNTs were selected for doping because of their larger effective surface area, with many sites available to adsorb gas molecules, and their hollow geometry that may be helpful to enhance the sensitivity and reduce the operating temperature. Furthermore, MWCNTs were reported to be sensitive to H_2, with good recovery times [27].

2. Experimental

2.1. Preparation of Materials

Commercial WO_3 powder was obtained from Merck and used without further purification. MWCNTs were grown by the thermal chemical vapor deposition (CVD) process. The catalyst layer of aluminium oxide (10 nm) and stainless steel (5 nm) was deposited on the silicon (100) substrates (Semiconductor Wafer Inc.) using reactive sputtering apparatus. The synthesis of MWCNTs was performed under a flow of acetylene/hydrogen at a ratio of 3.6:1 at 700 °C for 3 min. To obtain high-purity MWCNTs, the water-assisted selective etching technique [28] was applied after each CNT's growth stage. Water vapor (300 ppm) was introduced into the system by bubbling argon gas through liquid water at room temperature for 3 min. The sequence of acetylene/hydrogen and water vapor flows was repeated for five cycles. Based on the scanning electron microscopic (SEM) image, as shown in Figure 1, the diameter and length of the MWCNTs are ~35 nm and ~26 μm, respectively. The electrical conductivity of MWCNTs was ~75 S/cm, as measured by a four-point probe method at room temperature. In addition, high-resolution transmission electron microscopic (HR-TEM) imaging,

as shown in Figure 2, confirms that CNTs are multi-walled, with the width and number of walls being ~4.6 nm and 14, respectively. Thus, the spacing between two graphitic layers is ~0.33 nm, which is in good agreement with theoretical and experimental values.

Figure 1. SEM images of the produced MWCNTs grown by the CVD process.

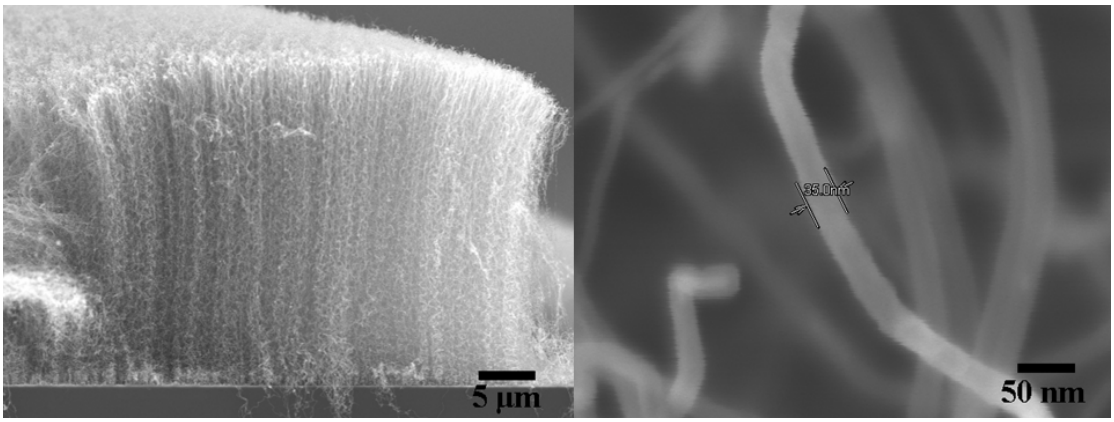

Figure 2. High resolution TEM image of the produced MWCNT grown by the CVD process.

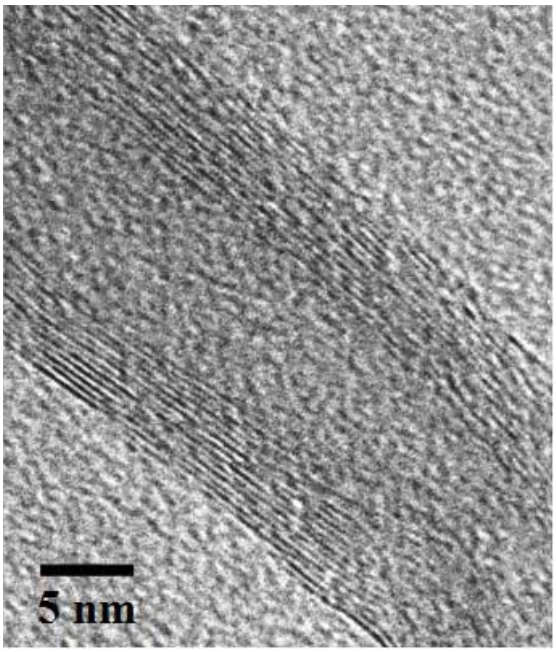

2.2. Fabrication of MWCNTs-doped WO_3 Thin Film

MWCNT-doped WO_3 thin film was fabricated by the E-beam evaporation technique onto Cr/Au interdigitated electrodes on an alumina substrate [29]. The target was prepared by mixing 99 wt% of WO_3 powder with 1 wt% of MWCNT powder using a grinder in a mortar for 30 min and then pelletizing with a hydraulic compressor. Deposition was performed at a pressure of 5×10^{-6} Torr in the evaporation chamber. The substrate was rotated and kept at 130 °C during the deposition in order to obtain a homogeneous thin film. The deposition rate was 2 Å/sec and the final film thickness was 150 nm, as controlled by a quartz crystal monitor. After E-beam evaporation, the film was

annealed at 500 °C for 3 h in air to stabilize the crystalline structure. In addition, an undoped WO_3 thin film was also fabricated using the same conditions for comparison.

2.3. Measurement of Gas Sensing

To evaluate the gas sensing properties of the thus prepared thin films, MWCNT-doped WO_3 and undoped WO_3 gas sensors were placed inside a stainless steel chamber and the resistance measured using a 8846A Fluke multimeter with 6.5 digit resolution. The gas sensing measurements were made within a dynamic flow system with control of sensor operating temperatures (200–400 °C) under variable gas concentrations (100–50,000 ppm). Hydrogen (H_2), ethanol (C_2H_5OH), methane (CH_4), acetylene (C_2H_2), and ethylene (C_2H_4) were used to test the sensing properties and selectivity of the thin films. The sample gas flow time and the clean air reference flow time were fixed at 5 min and 15 min, respectively. It should be noted that these switching interval was selected so that the resistance change is at least 90% of the saturated value. The sensor resistances were sampled and recorded every second using LabVIEW with a USB DAQ device for subsequent analyses.

3. Results and Discussion

3.1. Characterization of Thin Films

Surface morphology, particle size and crystalline structure of the films were characterized by SEM and TEM. Figure 3 shows the SEM surface morphology of MWCNT-doped WO_3 thin film deposited on an alumina substrate. It was seen that the film coated on the rough alumina substrate has approximate grain sizes ranging from 40 to 80 nm.

Figure 3. SEM image of MWCNT-doped WO_3 thin films on alumina substrate.

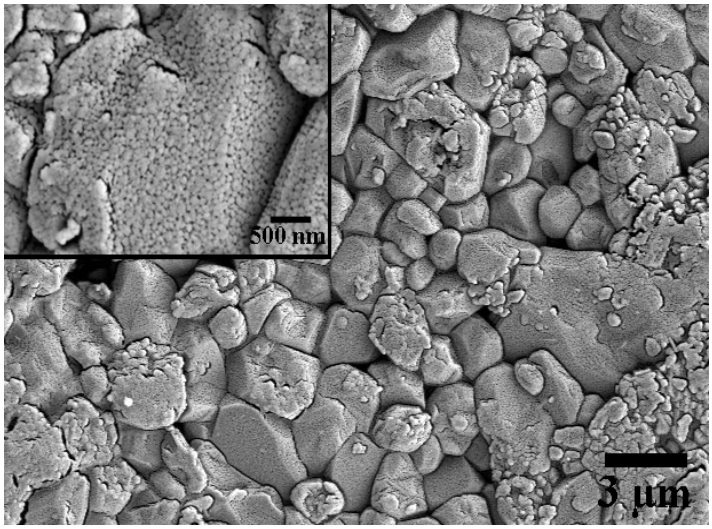

The nanometer grain size together with the roughness of the alumina substrate can enhance the gas sensitivity of thin films [30,31] because more gas adsorption sites are available due to the increased surface area and porosity. With the SEM resolution, CNT structure cannot be observed on the thin film surface. Therefore, TEM characterization was used to confirm CNT inclusion into the WO_3 film. It should be noted that copper TEM grid samples were loaded inside the evaporation chamber for sample

deposition at the same time as coating on the Cr/Au interdigitated electrodes. TEM observation clearly shows CNT inclusion into the nanocrystalline WO_3, while the electron diffraction pattern exhibits polycrystalline phase in the film, as shown in Figure 4a,b, respectively.

Figure 4. (a) High-resolution TEM image and **(b)** corresponding selected area diffraction pattern of MWCNT-doped WO_3 thin film.

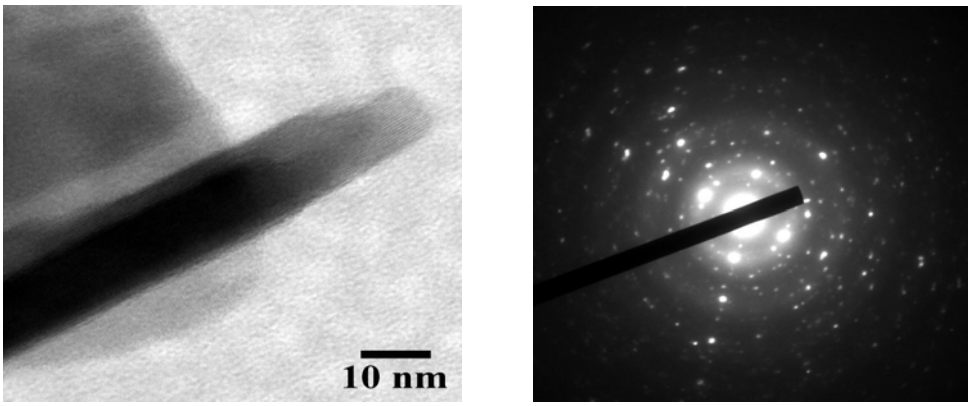

(a) (b)

The film morphology obtained in our study is in accordance with observations on nanocrystalline WO_3 films grown by other methods [32,33]. Doping of CNT does not change the phase or surface morphology of the film, but it may help form nanochannels in WO_3 films, leading to the enhancement of the sensitivity and reduction of the operating temperature.

3.2. Sensing Properties of Thin Films

The sensor response (S) of the thin films is defined as the percentage of resistance change:

$$S(\%) = \left(\frac{R_0 - R}{R_0} \right) \times 100 \quad (1)$$

where R_0 and R are the resistance of the thin films in pure air and test gas, respectively. Figure 5 shows the response of the undoped WO_3 and MWCNT-doped WO_3 thin films to 1,000 ppm H_2 at varying operating temperatures. It can be seen that the response of the films increases as the operating temperature increases up to 350 °C, and then decreases. The gas-sensing response increases with temperature in the 200–350 °C range because thermal energy helps the reactions involved overcome their respective activation energy barriers [34,35]. However, if the operating temperature becomes too high (*i.e.*, >350 °C), the adsorbed oxygen species at the sensing sites on the film surface will be diminished and less available to react with H_2 molecules [36], thereby limiting the film's response.

Figure 5. Sensing response to H_2 (1,000 ppm) at different operating temperatures.

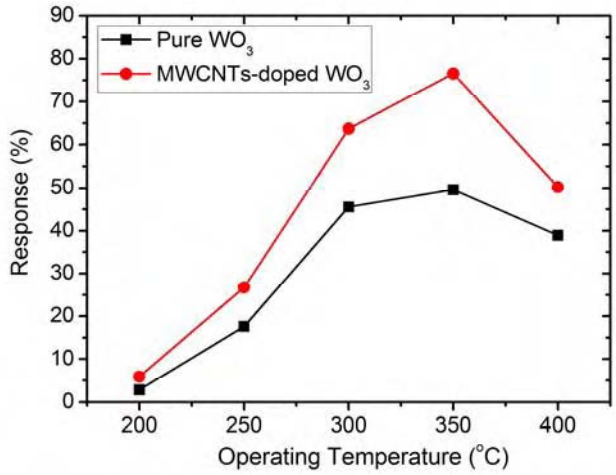

At any operating temperature, the sensor response of the MWCNT-doped WO_3 thin film is higher than that of the undoped WO_3 thin film. Specifically, at the optimum operating temperature (350 °C), MWCNT-doped WO_3 thin film yields a 26.9 % higher response than the undoped one. The doped sensor prepared in this work also shows higher response than the WO_3 films prepared by the sol–gel process [25].

Figure 6. Sensing response of the undoped WO_3 and MWCNT-doped WO_3 thin films to high H_2 concentrations (5,000–50,000 ppm) at the operating temperature of 250 °C.

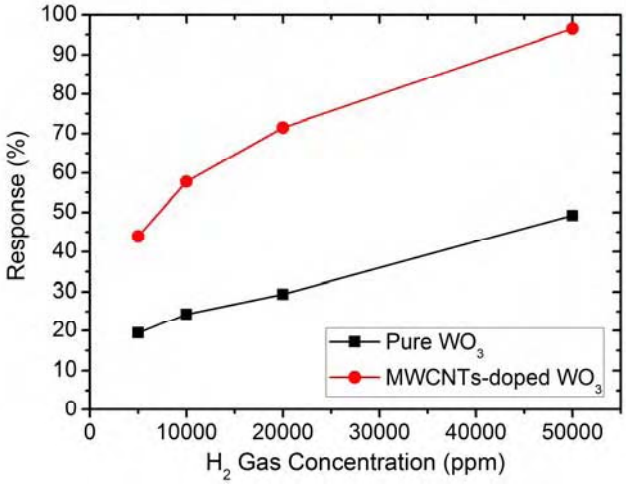

One major advantage of MWCNT-doped WO_3 thin film is that the sensor can be operated at a lower operating temperature (250 °C), especially if this sensor is used to measure the H_2 gas at higher concentrations (5,000–50,000 ppm). As shown in Figure 6, at such a concentration range, there are sufficient numbers of H_2 molecules available to react with the surface oxygen adsorption sites. It is also well-known that MWCNTs contribute to the reduction of sensor resistance of metal oxides [37] and the activation energy between the WO_3 surface and H_2 gas. The details of the sensing mechanisms of MWCNT-doped WO_3 thin films will be discussed in the next section.

To demonstrate the selectivity of the MWCNT-doped WO_3 thin film, its sensing response (at the operating temperature of 350 °C) to various gas vapors, namely H_2, C_2H_5OH, CH_4, and C_2H_2, was measured and plotted (Figure 7). It can be seen that MWCNT-doped WO_3 thin film exhibits a strong response to H_2, and much weaker responses to C_2H_5OH, CH_4, and C_2H_2. In particular, this thin film was found to be insensitive to C_2H_4 at the optimum operating temperature of 350 °C. It is therefore concluded that the MWCNT-doped WO_3 thin film exhibits high selectivity to H_2.

Figure 7. Sensing response of MWCNT-doped WO_3 thin film at the operating temperature of 350 °C to various concentrations of different gas vapors.

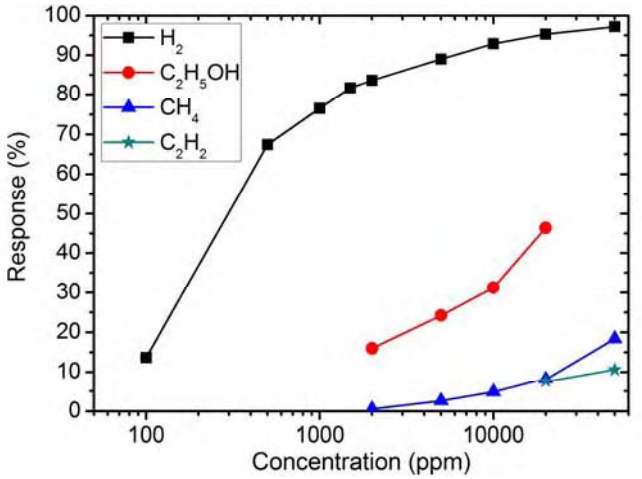

3.3. Sensing Mechanism of MWCNTs-doped WO_3 Thin Film

It is well known that WO_3 is an n-type semiconductor while CNT is a p-type semiconductor. MWCNT-doped WO_3 thin film can be either p-type or n-type semiconductors depending on the quantity of MWCNTs and the operating temperature [38]. In this work, the produced MWCNTs-doped WO_3 thin film behaves as an n-type semiconductor since the electrical conductivity of the film increases when reducing gases, *i.e.*, H_2, are absorbed by its surface. Doping of MWCNTs into the WO_3 matrix can introduce nanochannels and form p-n heterojunctions in the thin film. These nanochannels play an important role for gas diffusion. The gas molecules can easily transport into the gas-sensing layers leading to increasing sensitivity [39,40]. In addition, MWCNT-doped WO_3 thin film p-n heterojunctions could be formed at the interface between WO_3 and the MWCNTs [38,41]. When H_2 gas is exposed to MWCNT-doped WO_3 thin film, the widths of the depletion layers at the p-n heterojunctions can be modulated. The potential barriers at the interfaces or inside the WO_3 may be changed. This change of the depletion layer in the p–n heterojunctions of MWCNT-doped WO_3 thin film may explain the enhanced response of the film at low operating temperatures. Various oxygen species chemisorbed at the thin film surface such as O^{2-}, O_2^-, and O^- are available for catalytic reactions with H_2, thus depending on the temperature at the metal oxide surface [42]. At the operating temperature range of 200–400 °C, O^- is commonly chemisorbed. Consequently, the chemical reaction underlying the H_2 gas sensing in this study is given by [43]:

$$H_2 + O_{ads}^- \rightarrow H_2O + e^- \quad (2)$$

The adsorbed O^- on the thin film surface reacts with the H_2 gas yielding H_2O and releasing electrons which contribute to the current increase through the thin film that causes the electrical conductivity to increase.

4. Conclusions

MWCNT-doped WO_3 thin film was successfully prepared by the E-beam evaporation technique. The 1 wt% MWCNT-doped WO_3 thin film exhibits n-type semiconductor behavior of the polycrystalline phase. Doping with MWCNTs does not significantly change any phase or surface morphology of the film, but it introduces nanochannels and form p-n heterojunctions in the WO_3 matrix. The MWCNT-doped WO_3 thin film exhibits high selectivity and sensitivity to H_2 over a relatively wide range of concentrations (100-50,000 ppm). Moreover, it can operate at a relatively low temperature. This should be useful for developing high performance H_2 gas sensors. To our best knowledge, this is the first report on MWCNT-doped WO_3 hydrogen sensors prepared by the E-beam method.

Acknowledgements

Mahidol University and the National Science and Technology Agency are gratefully acknowledged for supports of this research. C.W. acknowledges the Commission on Higher Education for a Ph.D. scholarship under the program "Strategic Scholarships for Frontier Research Network". T.K. expresses his great gratitude to the Thailand Research Fund (BRG5180023) for a research career development grant.

References

1. Korotcenkov, G.; Han, S.D.; Stetter, J.R. Review of electrochemical hydrogen sensors. *Chem. Rev.* **2009**, *109*, 1402-1433.
2. Moriarty, P.; Honnery, D. Hydrogen's role in an uncertain energy future. *Int. J. Hydrogen. Energ.* **2009**, *34*, 31-39.
3. Momirlan, M.; Veziroglu, T.N. The properties of hydrogen as fuel tomorrow in sustainable energy system for a cleaner planet. *Int. J. Hydrogen. Energ.* **2005**, *30*, 795-802.
4. Árnason, B.; Sigfússon, T.I. Iceland—A future hydrogen economy. *Int. J. Hydrogen. Energ.* **2000**, *25*, 389-394.
5. Carcassi, M.N.; Fineschi, F. Deflagrations of H_2-air and CH_4-air lean mixtures in a vented multi-compartment environment. *Energy* **2005**, *30*, 1439-1451.
6. Penza, M.; Tagliente, M.A.; Mirenghi, L.; Gerardi, C.; Martucci, C.; Cassano, G. Tungsten trioxide (WO_3) sputtered thin films for a NO_x gas sensor. *Sens. Actuat. B Chem.* **1998**, *50*, 9-18.
7. Wang, X.; Miura, N.; Yamazoe, N. Study of WO_3-based sensing materials for NH_3 and NO detection. *Sens. Actuat. B Chem.* **2000**, *66*, 74-76.
8. Kim, T.S.; Kim, T.B.; Yoo, K.S.; Sung, G.S.; Jung, H.J. Sensing characteristics of dc reactive sputtered WO_3 thin films as an NO_x gas sensor. *Sens. Actuat. B Chem.* **2000**, *62*, 102–108.

9. Sawicka, K.M.; Prasad, A.K.; Gouma, P.I. Metal oxide nanowires for use in chemical sensing applications. *Sens. Lett.* **2005**, *3*, 31-35.
10. Tao, W.H.; Tsai, C.H. H_2S sensing properties of noble metal doped WO_3 thin film sensor fabricated by micromachining. *Sens. Actuat. B Chem.* **2002**, *81*, 237-247.
11. Frühberger, B.; Grunze, M.; Dwyer, D.J. Surface chemistry of H_2S-sensitive tungsten oxide films. *Sens. Actuat. B Chem.* **1996**, *31*, 167-174.
12. Hoel, A.; Reyes, L.F.; Heszler, P.; Lantto, V.; Granqvist, C.G. Nanomaterials for environmental applications: Novel WO_3-based gas sensors made by advanced gas deposition. *Curr. Appl. Phys.* **2004**, *4*, 547-553.
13. Ionescu, R.; Hoel, A.; Granqvist, C.G.; Llobet, E.; Heszler, P. Low-level detection of ethanol and H_2S with temperature-modulated WO_3 nanoparticle gas sensors. *Sens. Actuat. B Chem.* **2005**, *104*, 132-139.
14. Li, X.; Zhang, G.; Cheng, F.; Guo, B.; Chen, J. Synthesis, characterization, and gas-sensor application of WO_3 nanocuboids. *J. Electrochem. Soc.* **2006**, *153*, 133-137.
15. Xu, Y.; Tang, Z.; Zhang, Z.; Ji, Y.; Zhou, Z. Large-scale hydrothermal synthesis of tungsten trioxide nanowires and their gas sensing properties. *Sens. Lett.* **2008**, *6*, 938-941.
16. Neri, G.; Micali, G.; Bonavita, A.; Ipsale, S.; Rizzo, G.; Niederberger, M.; Pinna, N. Tungsten oxide nanowires-based ammonia gas sensors. *Sens. Lett.* **2008**, *6*, 590-595.
17. Llobet, E.; Molas, G.; Molinàs, P.; Calderer, J.; Vilanova, X.; Brezmes, J.; Sueiras, J.E.; Correig, X. Fabrication of highly selective tungsten oxide ammonia sensors. *J. Electrochem. Soc.* **2000**, *147*, 776-779.
18. Balázsia, C.; Wang, L.; Zayim, E.O.; Szilágyid, I.M.; Sedlackovác, K.; Pfeifera, J.; Tótha, A.L.; Goumab, P.I. Nanosize hexagonal tungsten oxide for gas sensing applications. *J. Eur. Ceram. Soc.* **2008**, *28*, 913-917.
19. Wang, U.; Pfeifer, J.; Balazsi, C.; Gouma, P.I. Synthesis and sensing properties to NH_3 of hexagonal WO_3 metastable nanopowders. *Mater. Manuf. Process.* **2007**, *22*, 773–776.
20. Berger, O.; Hoffmann, T.; Fischer, W.J.; Melev, V. Tungsten-oxide thin films as novel materials with high sensitivity and selectivity to NO_2, O_3, and H_2S. Part II: Application as gas sensors. *J. Mater. Sci.: Mater. Electron.* **2004**, *15*, 483-493.
21. Aroutiounian, V. Metal oxide hydrogen, oxygen, and carbon monoxide sensors for hydrogen setups and cells. *Int. J. Hydrogen. Energ.* **2007**, *32*, 1145-1158.
22. Ahmad, A.; Walsh, J. Development of WO_3-based thick-film hydrogen sensors. *ECS Trans.* **2006**, *3*, 141-152.
23. Ippolito, S.J.; Kandasamy, S.; Kalantar-zadeh, K.; Wlodarski, W. Hydrogen sensing characteristics of WO_3 thin film conductometric sensors activated by Pt and Au catalysts. *Sens. Actuat. B Chem.* **2005**, *108*, 154-158.
24. Hsu, W.C.; Chan, C.C.; Peng, C.H.; Chang, C.C. Hydrogen sensing characteristics of an electrodeposited WO_3 thin film gasochromic sensor activated by Pt catalyst. *Thin Solid Films* **2007**, *516*, 407-411.
25. Fardindoost, S.; Iraji-zad, A.; Rahimi, F.; Ghasempour, R. Pd doped WO_3 films prepared by sol–gel process for hydrogen sensing. *Int. J. Hydrogen. Energ.* **2010**, *35*, 854-860.

26. Nakagawa, H.; Yamamoto, N.; Okazaki, S.; Chinzei T.; Asakura, S. A room-temperature operated hydrogen leak sensor. *Sens. Actuat. B Chem.* **2003**, *93*, 468-474.
27. Samarasekara, P. Hydrogen and methane gas sensors synthesis of multi-walled carbon nanotubes. *Chin. J. Phys.* **2009**, *47*, 361-369.
28. Zhu, L.; Xiu, Y.; Hess, D.W.; Wong, C.P. Aligned carbon nanotube stacks by water-assisted selective etching. *Nano Lett.* **2005**, *5*, 2641–2645.
29. Wongchoosuk, C.; Wisitsoraat, A.; Tuantranont, A.; Kerdcharoen T. Portable electronic nose based on carbon nanotube-SnO_2 gas sensors and its application for detection of methanol contamination in whiskeys. *Sens. Actuat. B Chem.* **2010**, *147*, 392–399.
30. Ansari, Z.A.; Ansari, S.G.; Ko, T.; Oh, J.H. Effect of MoO_3 doping and grain size on SnO_2-enhancement of sensitivity and selectivity for CO and H_2 gas sensing. *Sens. Actuat. B Chem.* **2002**, *87*, 105-114.
31. Lee, D.S.; Nam, K.H.; Lee, D.D. Effect of substrate on NO_2-sensing properties of WO_3 thin film gas sensors. *Thin Solid Films* **2000**, *375*, 142-146.
32. Hussain, O.M.; Swapnasmitha, A.S.; John, J.; Pinto, R. Structure and morphology of laser-ablated WO_3 thin films. *Appl. Phys. A: Mater. Sci. Process.* **2005**, *81*, 1291-1297.
33. Ashrit, P.V. Dry lithiation study of nanocrystalline, polycrystalline and amorphous tungsten trioxide thin-films. *Thin Solid Films* **2001**, *385*, 81-88.
34. Shinde, V.R.; Gujar, T.P.; Lokhande, C.D. LPG sensing properties of ZnO films prepared by spray pyrolysis method: Effect of molarity of precursor solution. *Sens. Actuat. B Chem.* **2007**, *120*, 551-559.
35. Zeng, Y.; Zhang, T.; Wang, L.; Kang, M.; Fan, H.; Wang, R.; He, Y. Enhanced toluene sensing characteristics of TiO_2-doped flowerlike ZnO nanostructures. *Sens. Actuat. B Chem.* **2009**, *140*, 73-78.
36. Sahay, P.P.; Nath, R.K. Al-doped zinc oxide thin films for liquid petroleum gas (LPG) sensors. *Sens. Actuat. B Chem.* **2008**, *133*, 222-227.
37. Liang, Y.X.; Chen, Y.J.; Wang, T.H. Low-resistance gas sensors fabricated from multiwalled carbon nanotubes coated with a thin tin oxide layer. *Appl. Phy. Lett.* **2004**, *85*, 666-668.
38. Bittencourt, C.; Felten, A.; Espinosa, E.H.; Ionescu, R.; Llobet, E.; Correig, X.; Pireaux, J.J. WO_3 films modified with functionalised multi-wall carbon nanotubes: Morphological, compositional and gas response studies. *Sens. Actuat. B Chem.* **2006**, *115*, 33-41.
39. Sakai, G.; Matsunaga, N.; Shimanoe, K.; Yamazoe, N. Theory of gas-diffusion controlled sensitivity for thin film semiconductor gas sensor. *Sens. Actuat. B Chem.* **2001**, *80*, 125-131.
40. Hieu, N.V.; Duc, N.A.P.; Trung, T.; Tuan, M.A.; Chien, N.D. Gas-sensing properties of tin oxide doped with metal oxides and carbon nanotubes: A competitive sensor for ethanol and liquid petroleum gas. *Sens. Actuat. B Chem.* **2010**, *144*, 450-456.
41. Wei, B.Y.; Hsu, M.C.; Su, P.G.; Lin, H.M.; Wu, R.J.; Lai, H.J. A novel SnO_2 gas sensor doped with carbon nanotubes operating at room temperature. *Sens. Actuat. B Chem.* **2004**, *101*, 81-89.
42. Cheong, H.W.; Lee, M.J. Sensing characteristics and surface reaction mechanism of alcohol sensors based on doped SnO_2. *J. Ceram. Process. Res.* **2006**, *7*, 183-191.

43. Lupan, O.; Ursaki, V.V.; Chai, G.; Chow, L.; Emelchenko, G.A.; Tiginyanu, I.M.; Gruzintsev, A.N.; Redkin, A.N. Selective hydrogen gas nanosensor using individual ZnO nanowire with fast response at room temperature. *Sens. Actuat. B Chem.* **2010**, *144*, 56-66.

Journal of
Nanoscience and Nanotechnology
Vol. 11, 1–6, 2011

An Electronic Nose for Amine Detection Based on Polymer/SWNT-COOH Nanocomposite

Panida Lorwongtragool[1, 2], Anurat Wisitsoraat[3], and Teerakiat Kerdcharoen[4, *]

[1] *Materials Science and Engineering Programme, Faculty of Science, Mahidol University, Bangkok 10400, Thailand*
[2] *Faculty of Science and Technology, Rajamangala University of Technology, Suvarnabhumi, Nonthaburi 11000, Thailand*
[3] *Nanoelectronic and MEMS Lab, National Electronic and Computer Technology Center, Pathumthani 12120, Thailand*
[4] *Department of Physics and Center of Nanoscience and Nanotechnology, Faculty of Science, Mahidol University, Bangkok 10400, Thailand*

An electronic nose (e-nose) system based on polymer/carboxylic-functionalized single-walled carbon nanotubes (SWNT-COOH) was developed for sensing various volatile amines. The SWNT-COOH dispersed in the matrix of different polymers; namely, polyvinyl chloride (PVC), cumene terminated polystyrene-co-maleic anhydride (cumene-PSMA), poly(styrenecomaleic acid) partial isobutyl/methyl mixed ester (PSE), and polyvinylpyrrolidon (PVP), were deposited on interdigitated gold electrodes to make the gas sensors. The response of these sensors to volatile amines was studied by both static and dynamic flow measurements. It was found that all sensors exhibited behaviors corresponding to Plateau–Bretano–Stevens law ($R^2 = 0.81$ to 0.99) as the response to volatile amines. Real-world application was demonstrated by applying this e-nose to monitor the odor of sun-dried snakeskin gourami that was pre-processed by salting-preservation. This electronic nose can discriminate sun-dried fish odors with different stored days using a simple pattern recognition based on the principal component analysis (PCA).

Keywords: Electronic Nose, Volatile Amine, CNT/Polymer Gas Sensor, Fish Freshness Monitoring.

RESEARCH ARTICLE

1. INTRODUCTION

Volatile amines are presented with strong and characteristic odor, mostly realized as unpleasant and toxic, i.e., the smell of ammonia, dried fish, putrid flesh and urine, etc. Amines are produced by decomposition of amino acids in biological processes. Therefore, amine sensor can be used to assess the freshness of protein-containing foods[1–7] as well as contaminated environment[8] related to biological wastes. Spoiling fish typically generates several kinds of amines such as ammonia, trimethylamine (TMA), dimethylamine (DMA) (these volatile compounds are also known as Total Volatile Basic Nitrogen (TVB-N))[1–2] and histamine (biogenic amines).[9–10]

Nowadays electronic nose has become a well-known technology for quality assessment of foods or drinks.[11–13] Electronic nose (e-nose) is fast, portable, low-cost and reliable. In principles, an e-nose consists of an array of gas sensors working cooperatively to detect a wide range of gases. The sensor response patterns are then recognized in order to identify or discriminate specific odors. Gas sensors based on carbon nanotubes (CNT)/polymer composites measure the electrical response under room temperature. The nanocomposited CNT with various polymers have been demonstrated to detect selective gases at low concentrations.

In this work, we have developed a new electronic nose system for amine detection based on an array of polymer/CNT nanocomposite gas sensors. In general, the underlying mechanism of polymer/carbon nanotube gas sensors is based on percolation of analytic gases into the polymer matrix leading to a drop in electrical conductance caused by volumetric increase in the materials. In principles, the polymers used in this type of gas sensors are non-conducting. Therefore, carbon nanotubes are mixed into the polymer matrix to act as conducting channel. Diffusion of the analytic gases into the polymer increases the separation between the conducting channels, thus decreasing the conductivity of the materials. Based on the above-mentioned sensing principles, there are two major factors that control the sensitivity of this type of sensors; swelling capability of polymer and electron-donating

*Author to whom correspondence should be addressed.

capability of analytic gases into carbon nanotubes. Identification of amine molecules is performed by presenting a variety of polymeric matrices with non-specific chemical interactions in the sensor array combined with a simple pattern recognize algorithm such as principal component analysis (PCA).

In the case of optoelectronic nose, clear differences of a wide range of toxic industrial chemicals (TICs)[14] and volatile amines[15] at very low concentrations (below the a.k.a. permissible exposure limits or PEL) have been demonstrated. Although an optoelectronic nose provides more powerful gas identification, the detection capability is limited at only low concentration. Thus, the presence of the analytic gases at higher concentration can lead to non-reproducibility. In the case of polymer/CNT composites, it has been shown that a wider range of amine concentrations can be detected. Therefore, applications of this electronic nose can be realized in the food and agriculture sectors where amine gases are presented at higher concentrations, i.e., in the chicken and pig farms and in the example as provided in this paper.

The objectives of this study are to developed amine sensors based on CNT/polymer composites for an e-nose and to apply this e-nose for the evaluation of dried fish spoilage. Traditional dried snakeskin gourami (called "Salid fish" in Thailand), preserved by 1–2 days exposure to sunlight following salting fermentation was investigated on their putrid odor as often observed if the dried fish was not frozen or cooked within a period of time.

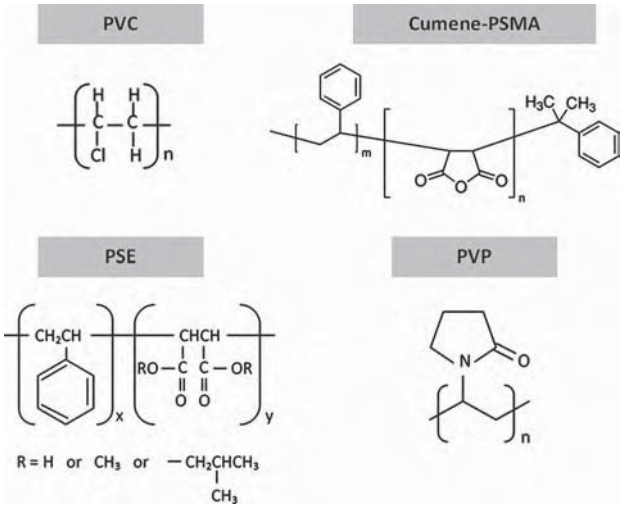

Fig. 1. Structures of polyvinyl chloride (PVC), cumene terminated polystyrene-co-maleic anhydride (cumene-PSMA), poly(styrene-co-maleic acid) partial isobutyl/methyl mixed ester (PSE), and polyvinylpyrrolidon (PVP).

2. EXPERIMENTAL DETAILS

2.1. Sensor Fabrication

The carboxylicfunctionalized single-walled carbon nanotube (SWNT-COOH) was used for producing the composites because it can be easily dispersed in solvents or polymer matrix due to its polarity.[16–17] Higher degree of mixing as present in the functionalized CNT/polymer sensors leads to increasing response and reversibility beyond the pristine CNT/polymer composites.[18–19] The purified SWNT-COOH (90 wt%) with 1–2 nm in diameter and 0.5–2.0 μm in length obtained from Cheap Tube Inc (www.cheaptubesinc.com) was dispersed in the polymer solutions of (i) PVC, (ii) cumene-PSMA, (iii) PSE and (iv) PVP (structures shown in Fig. 1). Each polymer was dissolved completely in 1 ml of the proper solvent (tetrahydrofuran, acetone, acetone and water, respectively). By optimizing the resulted device resistances to a kilo-ohms range, SWNT-COOH loading about 10–30 wt% with respect to the polymer content was blended into polymer solution and placed in the ultrasonic bath for 15 min to obtain uniform composite. Nanocomposite materials were deposited onto interdigitated electrodes by spin-coating and heated at 150 °C for 1 h to remove the residual solvent and impurities. The interdigitated electrodes were fabricated by E-beam evaporation of Cr/Au over alumina substrates through electroplated-Ni shadow masks. The thickness of Cr and Au layers are ~50 nm and ~200 nm, respectively. The width, spacing, and length of the IDE are approximately 100 μm, 100 μm, and 1 mm, respectively.

2.2. Measurement Setup

Gas sensing properties were investigated under static and dynamic flow measurement as illustrated in Figure 2. Both systems were measured at room temperature. To monitor sensor resistances under the static condition, single volatile amine was used each time to vary the concentrations in a 2000-cc chamber between 50–1000 ppm. Dimethylamine, dipropylamine, pyridine, and ammonium hydroxide were used as the vapor samples. Resistance of each sensor element was recorded for 1 min to obtain initial baseline and 5 min after injecting the sample.

Dynamic measurement was performed with real world samples to demonstrate that e-nose equipped with these sensors can determine the fish fressness based on amine detection. A simple e-nose was constructed using schematic diagram as shown in Figure 2. Sensor data were acquired through a USB DAQ device (NI USB-6008) from National Instruments. Nitrogen gas was used as reference and carrier gas to carry volatile species from the fish sample to reach to the sensor chamber. Solenoid valves were controlled to switch between reference gas and sample odors. An e-nose measurement consists of 4 reference-sample cycles, where the nitrogen gas was flowed directly through the sensor chamber for 7 min to obtain baseline and switched to flow through the sample container

RESEARCH ARTICLE

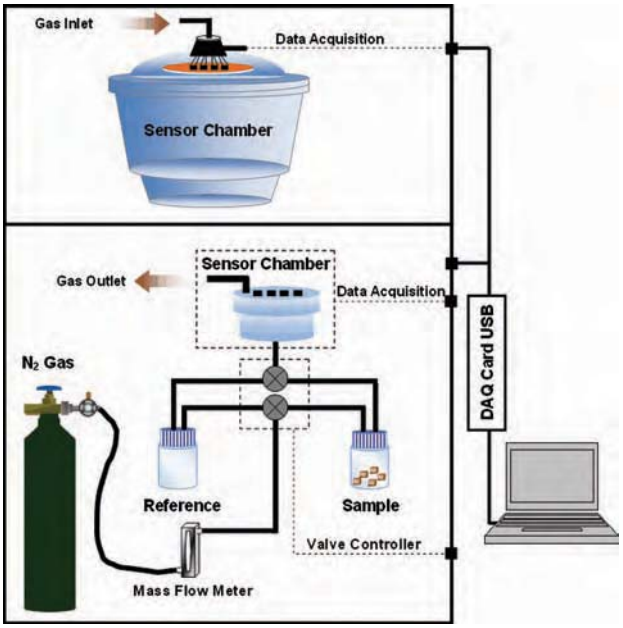

Fig. 2. Schematic diagram of the experimental setups for detecting volatile amines in the static system (top) and the dynamic flow system (below).

for another 1 min. The flow rate was controlled at 2.5 liters/min. The experiment was repeated for 3 times for each fish sample.

2.3. Sample Preparation

Sun-dried snakeskin gourami (*Trichopodus pectoralis*) were obtained from a local market as photographed in Figure 3. The fishes were sliced to remove the bones and cut into small pieces, then kept in glass bottles at room temperature. For e-nose measurement, only 5 g of the stored fishes were used. Odor measurements by e-nose were performed for four consecutive days.

2.4. Data Analysis

The minima and maxima values on the resistance curves obtained by switching between the reference and sample odors were extracted and used as the feature for data analysis. To avoid baseline inconsistency, the percentage change in resistance was used as detailed elsewhere.[20] In case of single component odor of amines, a power function known as the Plateau–Bretano–Stevens law[21–22] can be adopted to model the sensitivity.

$$F = kI^n \tag{1}$$

Where F is sensor responses to particular stimuli, I is odorant concentration, k and n are parameters.

For complex odors, i.e., the dried fishes, principle component analysis (PCA) was used to evaluate the recognized pattern in order to discriminate the freshness of the dried fish.

3. RESULTS AND DISCUSSION

Figure 4 shows the fabricated gas sensors. Under the ambient condition, the resistances of these sensors are 5 kΩ–35 kΩ.

Figure 5 plots the average percent change in resistance of the four sensors as exposed to dimethylamine dipropylamine, pyridine, and ammonium hydroxide under the static condition. It was found that the sensor response increases with the rising amine concentration. The power law in Eq. (1) was used to model this behavior and the results can then be simplified as given in Table I. The R-square (R^2) values of all sensors exceed the value of 0.81, which demonstrates that the Plateau–Bretano–Stevens law can be valid for all elements, especially for PVC/SWNT-COOH sensor response to dimethylamine ($R^2 = 0.99$). All sensors correspond to the exponent $n < 1$; therefore, the exponent is compressive and the sensor response increases slowly as the concentration increases.[22]

According to the results, it was shown that PSE/SWNT-COOH composite gas sensor yields the highest response to amine volatile compounds. The underlying mechanism of this type of sensors requires that the analytic gas must diffuse into the polymer matrix via some types of molecular interactions. In most cases, the analytic gases interact weakly with the polymer through physi-sorption (i.e., dipole–dipole or van der Waals interactions). Specifically, the molecular structure of PSE allows stronger interactions (such as chemi-sorption) with amine compounds through the ester and carboxylic groups, as shown in Figure 1. The strength of these interactions depends on the basicity of the amine compounds (dipropylamine (pKb = 3.09) > dimethylamine (pKb = 3.29) > ammonia (pKb = 4.75) > pyridine (pKb = 8.75)). Because dipropylamine presents

Fig. 3. Sun-dried snakeskin gourami from Bangnamphung floating market, Samutprakan province, Thailand.

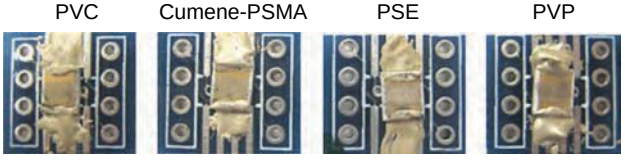

Fig. 4. Polymer/SWNT-COOH composites spin-coated on interdigitated electrodes: PVC, cumene-PSMA, PSE and PVP (left to right).

RESEARCH ARTICLE

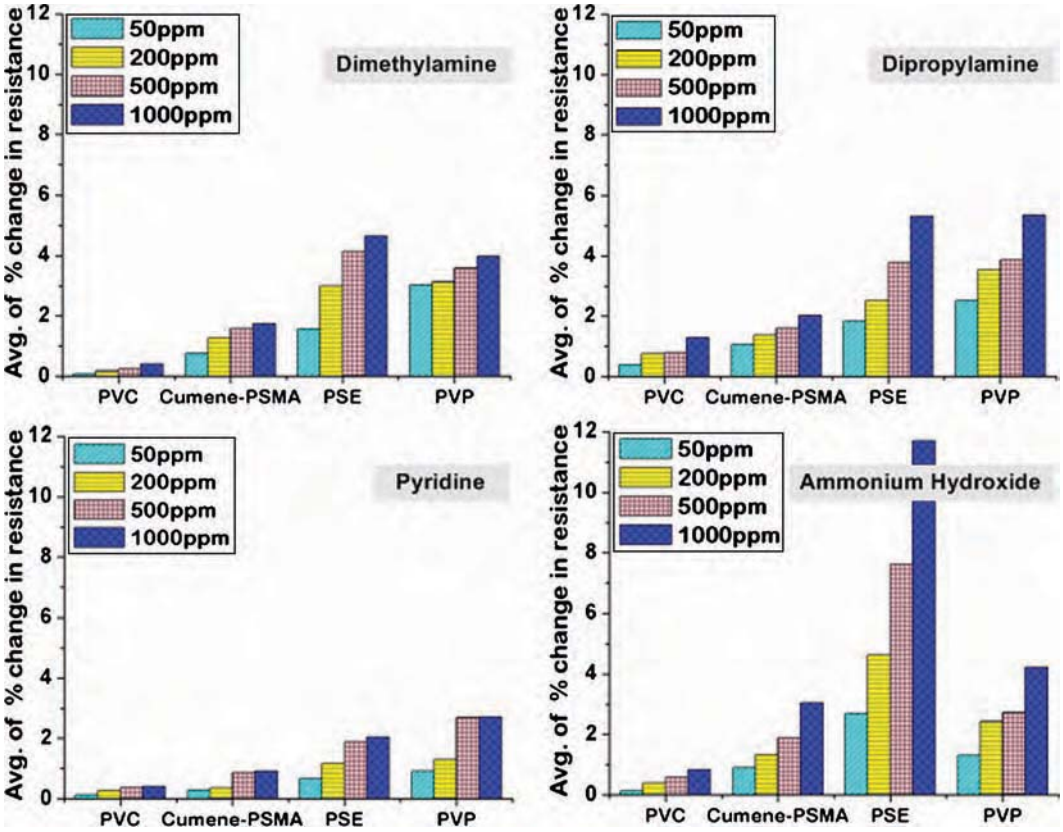

Fig. 5. The average of percent change in resistance of each sensor in static condition when exposed to dimethylamine, dipropylamine, pyridine, and ammonium hydroxide at the concentrations of 50–1000 ppm.

the highest basicity among other amines, it seems at first glance that this compound should exhibit highest sensing response with PSE. However, these secondary amines (dipropylamine and dimethyl amine) as well as pyridine have much lower mobility than ammonia to diffuse into the polymer matrix. As a result, the sensitivity of PSE to the amines is ranked as ammonia > dipropylamine > dimethylamine > pyridine), which is an outcome of the counterbalance between basicity and mobility of the volatile amines.

Table I. Parameters of power law models, Eq. (1) in each sensor element corresponding to amine measurements.

		Parameters		
Sensor	Amine compound	k	n	R^2
PVC/SWNT-COOH	Dimethylamine	0.01	0.59	0.99
	Dipropylamine	0.09	0.37	0.90
	Pyridine	0.03	0.38	0.92
	Ammonium hydroxide	0.01	0.61	0.96
Cumene-PSMA/ SWNT-COOH	Dimethylamine	0.27	0.28	0.95
	Dipropylamine	0.47	0.21	0.97
	Pyridine	0.05	0.44	0.82
	Ammonium hydroxide	0.18	0.39	0.94
PSE/SWNT-COOH	Dimethylamine	0.39	0.37	0.96
	Dipropylamine	0.43	0.35	0.95
	Pyridine	0.15	0.39	0.96
	Ammonium hydroxide	0.38	0.49	0.98
PVP/SWNT-COOH	Dimethylamine	2.06	0.09	0.81
	Dipropylamine	1.00	0.23	0.93
	Pyridine	0.18	0.40	0.88
	Ammonium hydroxide	0.32	0.37	0.94

Different capability of each polymer to swell the amine vapors leads to different sensitivity to each gas. Another factor that effects on the sensitivity is electron-donating properties of amine species to carbon nanotubes. Thus, the results indicate that the SWNT-COOH based on these polymers is a p-type semiconductor. In principles, e-nose should be made from an array of gas sensors that have different selective gases. By measuring a complex odor such as the sundried snakeskin gourami, pattern recognition is required to understand the data obtained from the measurement. Figure 6 shows the response of each sensor to the odor of the fish samples. A reversible behavior was observed in all sensors. A major obstacle for polymer composite gas sensors is well recognized as their poor stability. The efficiency of such sensors often decreases after repetitive usages. Moreover, thick sensing film may confine adsorbed volatile molecules within the polymer matrix. Therefore, optimization of the flow rate and measurement time must be optimized in order to maintain the consistency of the extracted features.[23]

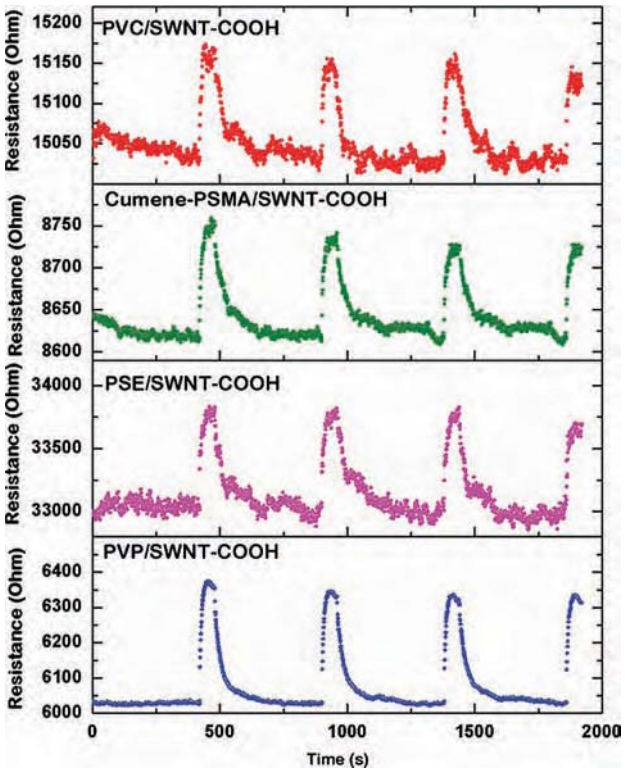

Fig. 6. The typical resistance changes with time of four sensors to sun-dried fish odor.

Figure 7 plots the sensor responses to the fish sample at different storage days (1–4 days). The increasing response from the 1st to 4th day indicates increasing amine vapors in the sample during that period. The principal component analysis of these data was performed and plotted in Figure 8. The PCA results show 80.67% and 16.73% of variance within the first and second components (PC1 and PC2) which implies that visualization of these data on 2D plot is highly relevant and e-nose made of these 4 sensors is sufficient to discriminate these samples. Data analysis by PCA can identify 4 groups of data based on their storage time (1 to 4 days).

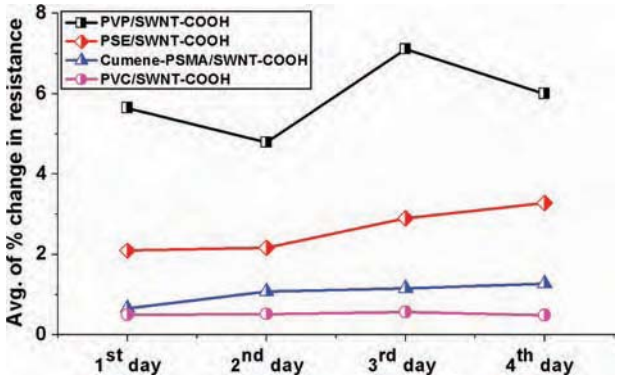

Fig. 7. The average of percent change in resistance of each sensor to volatile of the sun-dried snakeskin gourami between 1 to 4 days.

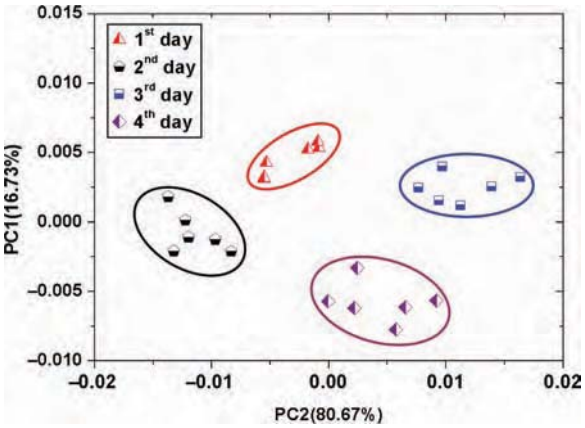

Fig. 8. The score plot of PCA for the sun-dried snakeskin gourami between 1 to 4 days.

4. CONCLUSION

In this paper, we have demonstrated that the electronic nose based on polymer/SWNT-COOH composite can identify the states of sun-dried snakeskin gourami by using a simple pattern recognition based on the principal component analysis (PCA). Volatile amines generated during the spoilage in many kinds of fish were shown in literatures to contain amine species known as Total Volatile Basic Nitrogen (TVB-N). Analytical examination of four single amine components with concentration range 50–1000 ppm indicates that the sensor response obeys the Plateau–Bretano–Stevens power law ($R^2 \geq 0.81$). The sensor based on PSE/SWNT-COOH film showed the best response. All sensors exhibit the behavior of *p*-type semiconductor. It is suggested that the sensor response is determined by two factors; the swelling capability of the polymer matrix and the electron-donating capability of amine to carbon nanotube.

Acknowledgments: This work was supported by Mahidol University and the National Science and Technology Agency. A research career development grant from the Thailand Research Fund (BRG5180023) to TK and a CHE-Ph.D.-SW-NEU scholarship from the Commission of Higher Education to PL are acknowledged.

References and Notes

1. A. Pacquit, K. T. Lau, H. McLaughlin, J. Frisby, B. Quilty, and D. Diamond, *Talanta* 69, 515 **(2006)**.
2. M. O'Connell, G. Valdora, G. Peltzer, and R. M.Negri, *Sens. Actuators B* 80, 149 **(2001)**.
3. N. E. Barbri, E. Llobet, N. E. Bari, X. Correig, and B. Bouchikhi, *Mater. Sci. Eng. C* 28, 666 **(2008)**.
4. Z. Zhang, J. Tong, D. Chen, and Y. Lan, *Journal of Bionic Engineering* 5, 67 **(2008)**.
5. C. D. Natale, G. Olafsdottir, S. Einarsson, E. Martinelli, R. Paolesse, and A. D'Amico, *Sens. Actuators B* 77, 572 **(2001)**.
6. J. Chantarachoti, A. C. H. Oliveira, B. H. Himelbloom, C. A. Crapo, and D. G. Mclachlan, *J. Food Sci.* 71, S414 **(2006)**.

RESEARCH ARTICLE

7. N. E. Barbria, J. Mirhisse, R. Ionescu, N. E. Bari, X. Correig, B. Bouchikhi, and E. Llobet, *Sens. Actuators B* 141, 538 **(2009)**.

8. J. Q. Ni, A. J. Heber, C. A. Diehl, and T. T. Lim, *J. agric. Engng Res.* 77, 53 **(2000)**.

9. M. L. N. E. Dapkeviciusa, M. J. Robert Nouta, F. M. Romboutsa, J. H. Houben, and W. Wymenga, *Int. J. Food Microbiol.* 57, 107 **(2000)**.

10. A. Lebiedzifiska, H. Lamparczyk, Z. Ganowiak, and K. I. Eller, *Z Lebensm Unters Forsch* 192, 240 **(1991)**.

11. E. Schaller, J. O. Bosset, and F. Escher, *Lebensm.-Wiss. u.-Technol* 31, 305 **(1998)**.

12. H. Yu, J. Wang, C. Yao, H. Zhang, and Y. Yu, *LWT-Food Science and Technology* 41, 1268 **(2008)**.

13. P.-M. Schweizer-Berberich, S. Vaihinger, and W. Giipel, *Sens. Actuators B* 18–19, 282 **(1994)**.

14. S. H. Lim, L. Feng, J. W. Kemling, C. J. Musto, and K. S. Suslick, *Nature Chemistry* 1, 562 **(2009)**.

15. Z. Tang, J. Yang, J. Yu, and B. Cui, *Sensor* 10, 6463 **(2010)**.

16. Y. Lin, M. J. Meziani, and Y. P. Sun, *J. Mater. Chem.* 17, 1143 **(2007)**.

17. T. Ramanathan, H. Liu, and L. C. Brinson, *J. Polym. Sci. B: Polym. Phys.* 43, 2269 **(2005)**.

18. B. Philip, J. K. Abraham, A. Chandrasekhar, and V. K. Varadan, *Smart Mater. Struct.* 12, 935 **(2003)**.

19. J. K. Abraham, B. Philip, A. Witchurch, V. K. Varadan, and C. C. Reddy, *Smart Mater. Struct* 13, 1045 **(2004)**.

20. C. Wongchoosuk, M. Lutz, and T. Kerdcharoen, *Sensors* 9, 7234 **(2009)**.

21. A. Szczurek and M. Maciejewska, *Sens. Actuators B* 106, 13 **(2005)**.

22. V. V. Kamadia, Y. Yoon, M. W. Schilling, and D. L. Marshall, *J. Food Sci.* 71, S193 **(2006)**.

23. T. C. Pearce, S. S. Schiffman, H. T. Nagle, and J. W. Gardner, Handbook of Machine Olfaction: Electronic Nose Technology, Wiley-VCH, Weinheim, **(2003)**, p. 325.

Received: 30 December 2009. Revised/Accepted: 30 August 2010.

Journal of
Nanoscience and Nanotechnology
Vol. 11, 1–6, 2011

An Artificial Nose Based on M-Porphyrin (M = Mg, Zn) Thin Film and Optical Spectroscopy

Sumana Kladsomboon[1], Sirapat Pratontep[2], Theeraporn Puntheeranurak[3, 4], and Teerakiat Kerdcharoen[1, 4, *]

[1] *Department of Physics and Center of Nanoscience, Faculty of Science, Mahidol University, Bangkok 10400, Thailand*
[2] *College of KMITL Nanotechnology, King Mongkut's Institute of Technology Ladkrabang, Chalongkrung Rd., Ladkrabang, Bangkok 10520, Thailand*
[3] *Department of Biology and Center of Nanoscience, Faculty of Science, Mahidol University, Bangkok 10400, Thailand*
[4] *NANOTEC Center of Excellence at Mahidol University, National Nanotechnology Center, Thailand*

Artificial nose has recently become an emerging instrument for quality assurance in the food industry. These paper present the optical gas sensors based on Magnesium-5,10,15,20-tetra phenyl-porphyrin (MgTPP) and Zinc-5,10,15,20-tetra phenyl-porphyrin (ZnTPP) thin films and their application as an artificial nose. Based on the measurement of optical absorbance response using a general UV-Vis spectroscopy, this artificial nose was tested to discriminate various volatile organic compounds (VOCs) and Thai beverages. Atomic force microscopy (AFM) and X-rays diffraction (XRD) were used to confirm the polycrystalline structure of the sensing materials. Density functional theory (DFT) calculations reveal that MgTPP interacts more strongly with the VOCs than ZnTPP, especially with methanol. The classification results of VOCs and Thai beverage vapors using the principal component analysis indicate that both MgTPP and ZnTPP-based artificial noses can be an efficient tool for quality assurance of alcoholic beverages.

Keywords: Gas Sensor, Porphyrin-Based Sensor, Optical Sensor.

RESEARCH ARTICLE

1. INTRODUCTION

Metal porphyrins (MP) are organic semiconductor materials able to adsorb gas molecule at the central metal atom or on the conjugated ¶-electron circumference.[1] The electrical and optical properties of MP are strongly induced by electron donors and acceptors.[2] As a result, MP has become a versatile material for gas sensor because many transducing techniques are allowed such as electrical,[3] optical and mass transduction.[4] In particular, the MP-based optical sensors provide many advantages over metal oxide-based sensors. Optical transducing is a rather convenient measurement method which may be operated at room temperature. Optical absorption spectra also yield much more informative and specific results with regards to chemical types than chemoresistive sensors. Only a single type of MP materials can be applied to make a device that can behave as an array of sensors.[5] We have previously shown that MgTPP and ZnTPP thin films can detect various volatile organic compounds (VOCs) based on UV-Vis spectroscopy.[6, 7] In this paper, we demonstrate the potentials of these sensor materials for an artificial nose system aimed at the beverage industry.

In this work, the spin-coating technique was employed to fabricate MgTPP and ZnTPP thin films, followed by X-ray diffraction (XRD) and atomic force microscopy to investigate the microstructure of the films. An artificial nose based on optical absorption change was constructed by housing the films in a flow chamber installed in between the light source and the detector probe of a UV-Vis spectrophotometer. The sensing properties were tested with various VOCs, namely, alcohols, acetone (5% aq.), acetic acid (5% aq.), methyl benzoate (5% aq.), and commercial alcoholic beverages. Theoretical calculations based on the density functional theory (DFT) were used to provide the understanding of VOCs-sensor interactions.[8, 9]

A pattern recognition technique based on the principal component analysis (PCA) has been demonstrated to classify many odors, such as alcohols, octane, toluene, and methylethylketon in the artificial noses.[10, 11] In addition, PCA was successfully used in colorimetric sensor array to describe the soft drinks[12] and portable E-nose based on CNT-SnO_2 gas sensors to describe the contamination of methanol in whisky.[13] To demonstrate the discrimination

*Author to whom correspondence should be addressed.

power of the MgTPP and ZnTPP thin films and the corresponding electronic nose, PCA has been employed to explore the data distribution and classify the samples.

2. MATERIALS AND METHODS

2.1. Experimental Details

MgTPP and ZnTPP were obtained from Sigma-Aldrich and Silpakorn University (synthesized by Dr. Radchada Buntem), respectively. MgTPP and ZnTPP were dissolved in chloroform at concentration of 0.017 M and 0.007 M, respectively. The solutions were subsequently spin-coated onto glass substrates at 1000 rpm for 30 seconds. A previous work has shown that improvements in the MgTPP gas sensing properties could be achieved by thermal annealing.[11] Therefore, MgTPP spin-coated thin films were placed in a furnace under the argon atmosphere, heated at the rate of 5 °C per minute to reach 280 °C and then allowed to cool down for 3 hours. The optical absorption spectra of thin films were recorded at the normal incidence in the range of 300–800 nm by the Jenway UV-Vis Spectrophotometer.

The gas sensing capability of the metal-tetra phenylporphyrin films have been investigated under the dynamic gas flow through a home built stainless steel chamber, equipped with quartz windows for optical measurements. Nitrogen (99.9%) gas was used as the reference and carrier gas to conduct headspace vapor from the sample bottle. The sample bottle was immersed in a heat bath controlled at 25 °C. The gas flow was switched between the reference and the vapor sample every 10 minutes. The measurements of each VOC consist of 5 alternating cycles between the reference and the sample. The experiment was repeated for at least another two times on each VOC.

2.2. Computational Method

DFT method was applied to investigate the interactions energy between VOCs and the sensing materials. The initial structures were constructed based on PM3 semi-empirical technique. Then the geometries were optimized using DFT calculations at the B3LYP/6-31G* level in the GAUSSIAN 03 program suite.[14] The interaction energies between the VOCs and the sensing molecules were calculated by varying the distance between the oxygen atom of each VOC molecules and the central metal of the sensing molecules. The interaction energies of MP with one and two molecules of VOC were compared. The interaction energy between the sensing material and gas molecule was calculated by Eq. (1):

$$E_{\text{Int}} = [E_{\text{MP+VOC}} - (E_{\text{MP}} + E_{\text{VOC}})] \quad (1)$$

where E_{Int} is the interaction energy between a sensing molecule and a VOC molecule. $E_{\text{MP+VOC}}$ denotes the total energy of the interacting pair. E_{MP} and E_{VOC} represent the total energies of the sensing and the VOC molecules, respectively.

3. RESULTS AND DISCUSSION

3.1. Optical Measurements and Sensing Characteristics

The absorption spectra of the MgTPP films were signified by the intense B band and Q band, as shown in Figure 1. MgTPP exhibits the B band peak at 438 nm and the Q band peaks at 570 and 610 nm. After thermal annealing, the B band intensity became lowered. In the case of ZnTPP, the B band peak at 436 nm and the Q band peaks at 555 and 600 nm are observed and the total absorbance also decreased after thermal annealing. The annealing process should therefore produce similar structural changes in both MgTPP and ZnTPP films, which has been explained to be a result of thermally-induced crystallization.[15] However, our previous study[11] found that the annealing process the annealed MgTPP films yielded higher responses to methanol vapor than the as spin-coated films, whereas the spin-coated ZnTPP films presented stronger methanol response than the treated films. So in this work, we compared the gas sensing properties between annealed MgTPP films and as spin-coated ZnTPP films.

The absorption spectra of each porphyrins can be related to an energy gap between the highest occupied molecular orbital (HOMO) and the lowest unoccupied molecular orbital (LOMO).[16] In a presence of an interacting gas molecule, the energy gap is affected, which leads to changes in the optical absorbance. The sensing response to VOCs is based on the measurement of absorptionchange duringthe gas exposure ($|A - A_0|$, where A and A_0 are the absorption spectra of the sample and reference gas. Hence, the absorption spectra were divided into six regions based

change to : absorption change

add round bracket

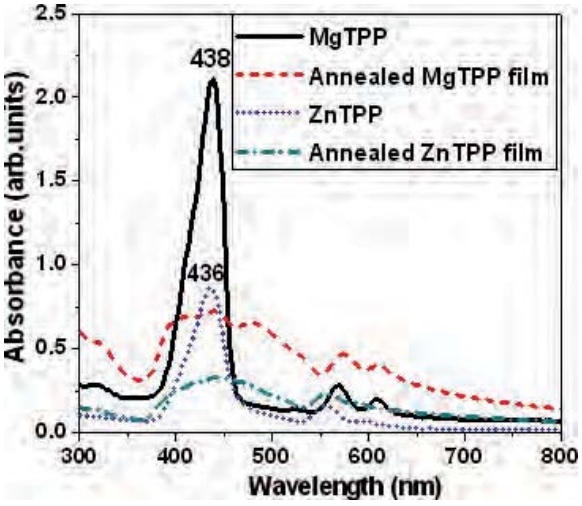

Fig. 1. Optical absorption spectra of the MgTPP and ZnTPP thin films.

RESEARCH ARTICLE

on the response to methanol because the sensing films show highest response to this gas. Therefore, the absorption change within each spectral region indicates sensitivity to each VOC relative to the methanol. For MgTPP, the spectral regions are R1: 300–370, R2: 370–410, R3: 410–490, R4: 490–555, R5: 555–610 and R6: 610–800 nm. For ZnTPP, the spectral regions are R1: 300–360, R2: 360–425, R3: 425–460, R4: 460–550, R5: 550–615 and R6: 615–800 nm. The delocalized π-electron system near the central metal atom in porphyrins is an important reason for VOC detection. The interaction of porphyrin and VOC affects the π–π^* interaction and the absorption spectra variation came from an increasing density in the electronic levels available for π–π^* transitions.[17] The gas sensing responses (S) were calculated from Eq. (2):

$$S = \Delta A / A_{\text{Base}} \tag{2}$$

where ΔA is difference of the integrated area within a specific range of absorption spectra between the sample (A) and reference (A_0) and A_{Base} is the total integrated area of absorption spectra before flowing gas.

Figure 2 shows the average gas sensing of MgTPP and ZnTPP film to 10 mol% of alcohol vapor in nitrogen gas. Both MgTPP and ZnTPP films express more sensing response to methanol than other alcohols. It can be seen that MgTPP is more selective to methanol comparing to ZnTPP. Thus, ZnTPP expresses higher response to ethanol and isopropyl alcohol than MgTPP. In Figure 2, the treated MgTPP films showed the molecular crystallization and the increasing of the grain size. The average roughness for MgTPP spin-coated film was about 2.83 nm. After thermal treatments, the MgTPP grain size can be approximated from the roughness to be 41.7 nm and the grain sizes of the treated MgTPP films is larger than ZnTPP spin coated film, showing the average roughness about 15 nm. The thickness of MgTPP and ZnTPP films are approximately 200 and 170 nm, respectively. Furthermore, in Figure 3, the as spin-coated ZnTPP film shows stronger responses than MgTPP in Region 2 for all VOCs. The strongest response for both porphyrin sensors corresponds to the Soret band which is located at 438 and 436 nm, indicating the π–π^* transition between bonding and anti-bonding molecular orbital in porphyrin compound.[8]

The structure of porphyrins powder and film were investigated by XRD (Cu Kα radiation, $\lambda = 1.5418$ nm) as shown in Figure 4. The intensity peaks at 2θ equal to 11° and 13° for all films are the effect of the glass slide substrate. For MgTPP, the diffraction peak of the annealed film occurs at 18.7°, which is absent in the non-annealed

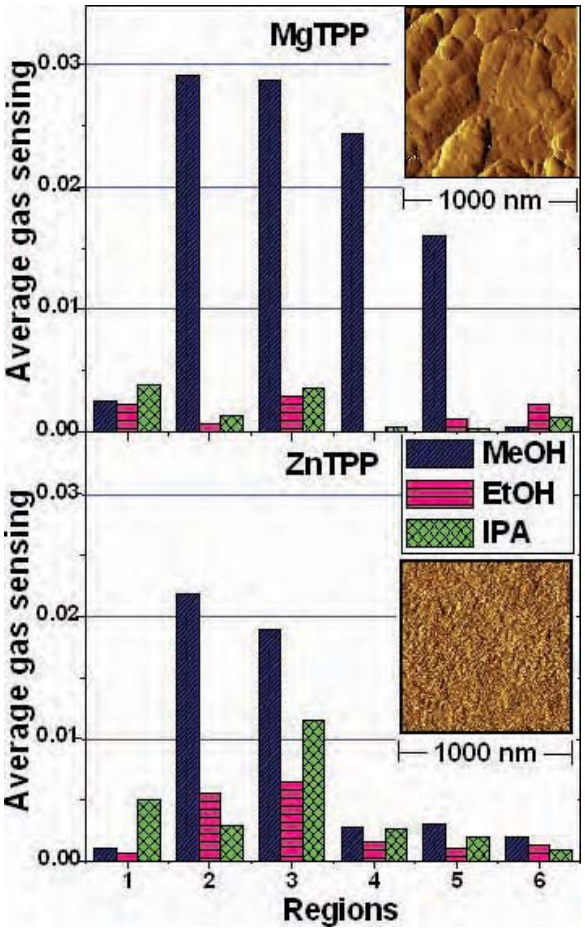

Fig. 2. The average gas sensing and DFM images in top views of MgTPP annealed film and ZnTPP spin coated film.

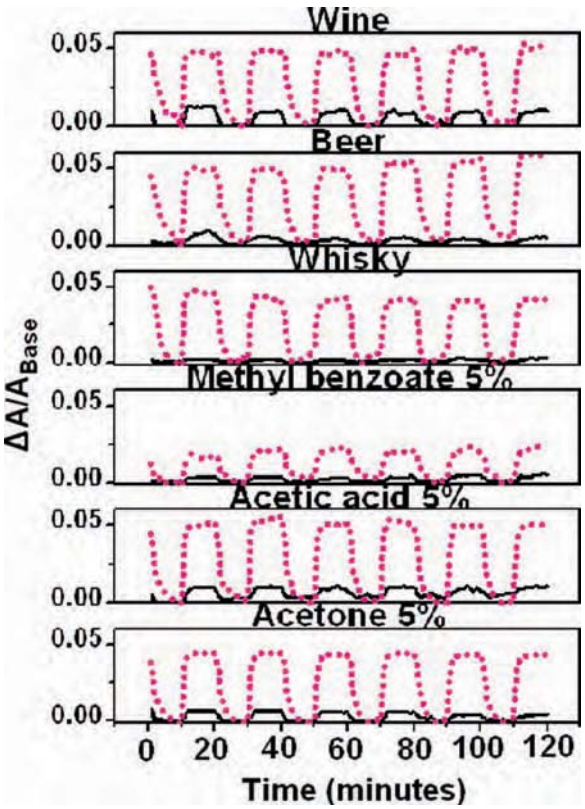

Fig. 3. The typical dynamic responses of VOCs and Thai beverages vapor of MgTPP treated film in Region 1 (solid line) and ZnTPP in Region 2 (dotted line).

RESEARCH ARTICLE

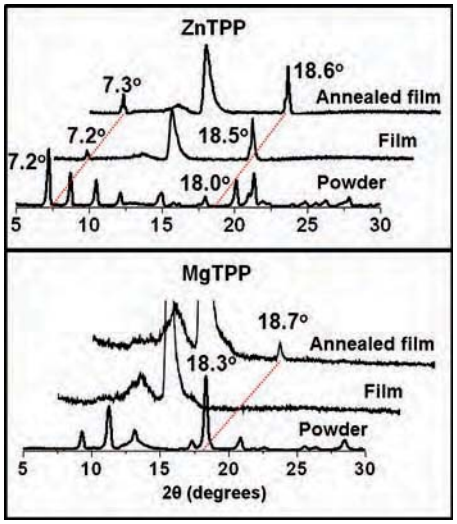

Fig. 4. The XRD patterns of MgTPP and ZnTPP compounds.

film. This peak corresponds to an interplanar distance (d) of 4.73 nm. This peak is also related to the main peak of MgTPP powder located at 18.3°. For ZnTPP, there is the diffraction peaks of both spin coated and annealed films. The diffraction peaks of spin coated film are observed at 7.2° and 18.5° and the diffraction peaks of annealed film shift to 7.3° and 18.6°, which corresponds to an interplanar distance (d) of 12.07 and 4.76 nm, respectively. In addition, the absorption spectra shifts of annealed MgTPP and ZnTPP films in Figure 1 were explained by an increase in diffraction peak intensities after thermal annealing.

3.2. Principal Component Analysis (PCA)

The PCA data sets were calculated from the average $\Delta A/A_{\text{Base}}$ values of the six wavelength regions (Region 1 to Region 6). Based on this methodin Figure 5, both sensors separated the result from the mixed VOCs solution in water such as methyl benzoate, acetone and acetic acid. But some overlap data plot between acetone and methyl benzoate area for MgTPP is caused by the low gas sensing responses of MgTPP (see in Fig. 3). So we can confirm that ed on a single type of organic c fficiency sensor. Moreove, ZnTPP had more efficiency to separate three types of alcohol beverages namely, whisky (40%), wine (12.5%) and beer (6.4%).

change to :
Moreover

3.3. DFT Calculations

DFT was used to predict and explain the gas-sensing characteristic of the organic compound. The lowest interaction

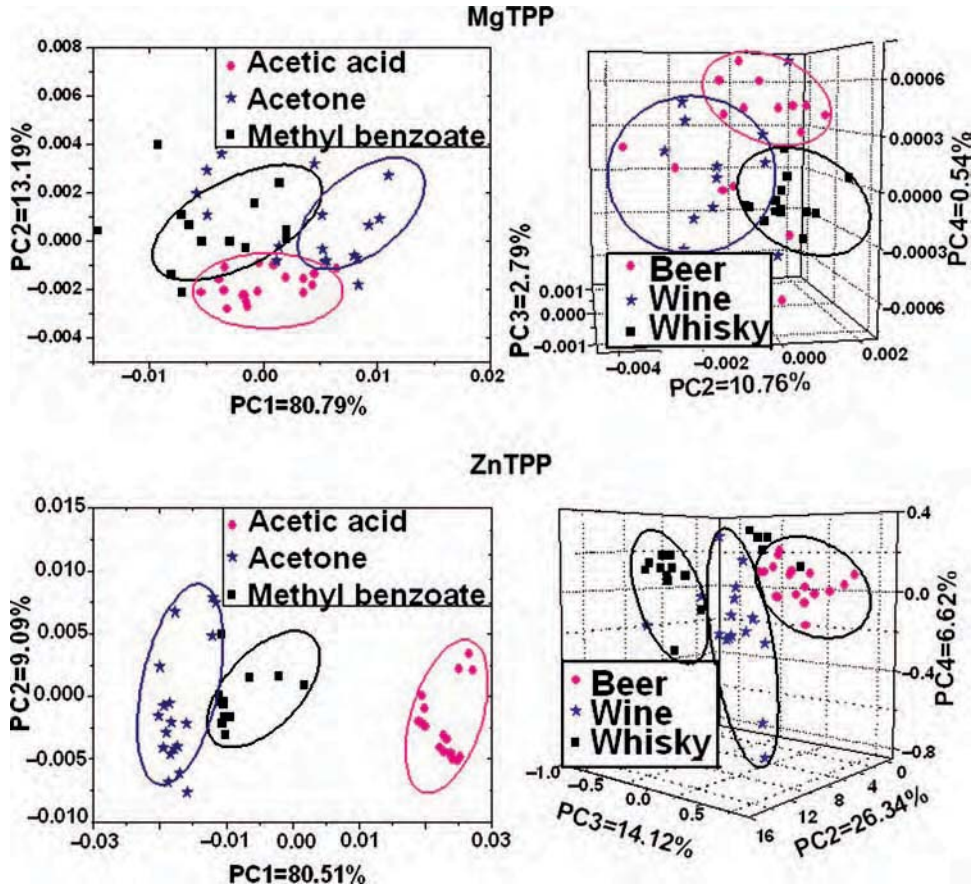

Fig. 5. PCA score plots related to the response of the array optical sensor corresponding to MgTPP and ZnTPP thin film.

RESEARCH ARTICLE

delete:atomic site

Table I. The interaction energies per 1 VOC molecule; ΔE_{Int} (kcal/mol) at the optimized distance; D (Å), change in energy gap (MgTPP = 2.82 eV and ZnTPP = 2.91 eV); ΔE_g (eV), and the change in NBO charge: for MgTPP at magnesium (1.70153 a.u.), nitrogen (−0.73441 a.u.); for ZnTPP at zinc (1.61282 a.u.), nitrogen (−0.71875 a.u.); for VOCs at oxygen atomic site (methanol; O − 0.741 a.u., ethanol; O − 0.759 a.u. and isopropanol; O − 0.753 a.u., acetone; O − 0.540 a.u., acetic acid; O − 0.591 a.u. and methyl benzoate; O − 0.599 a.u.) ~~atomic site.~~

	VOC 1 molecule			VOC 2 molecules			Delta NBO charge of VOC 1 molecule		
Interaction of	D	ΔE_{Int}	ΔE_g	D	ΔE_{Int}	ΔE_g	Metal	O	N
MgTPP with									
Methanol	2.375	−9.92	0.105	2.25	−10.29	0.097	+0.001	−0.045	+0.024
Ethanol	2.50	−8.37	0.098	2.50	−7.99	0.098	+0.002	−0.041	+0.022
Isopropanol	2.25	−7.83	0.102	2.50	−7.74	0.098	+0.003	−0.040	+0.023
Acetone	2.375	−7.61	0.117	2.25	−7.41	0.097	+0.001	−0.065	+0.028
Acetic acid (at –O bond)	2.375	−7.91	0.099	2.25	−7.25	0.097	+0.004	−0.060	+0.026
Methyl benzoate (at –O bond)	2.375	−7.59	0.099	2.375	−7.62	0.097	+0.006	−0.062	+0.027
ZnTPP with									
Methanol	2.375	−5.79	0.121	2.375	−5.66	0.101	+0.036	−0.046	+0.010
Ethanol	2.50	−5.66	0.104	2.625	−4.95	0.102	+0.031	−0.035	+0.007
Isopropanol	2.50	−5.97	0.103	2.625	−9.87	0.102	+0.031	−0.039	+0.010
Acetone	2.50	−4.08	0.109	2.625	−3.38	0.102	+0.034	−0.047	+0.010
Acetic acid (at –O bond)	2.50	−3.89	0.114	2.50	−3.60	0.101	+0.034	−0.048	+0.011
Methyl benzoate (at –O bond)	2.50	−4.11	0.102	2.625	−3.99	0.101	+0.037	−0.056	+0.011

energies from calculation method indicated that MPs present the stable structure with VOCs molecule in the optimized site. The interaction energies and the change in HOMO-LUMO energy gap of MTPP with one VOC molecule and two VOC molecules in Table I indicate that MTPP have the high interaction energies and the higher change in energy gap when it interacts with 1 VOC molecule. Both optical gas sensors indicated the strongest interactions with methanol, about −9.92 kcal/mol and −5.79 kcal/mol for MgTPP and ZnTPP, respectively, as shown Table I. This computational result agrees with the experiment results which measured alcohol sensing at the same molar concentration (in Fig. 2). Amongst ethanol, methanol and iso-propanol, both the MgTPP and ZnTPP films exhibit the strongest optochemical responses to methanol. This seems to be in accordance with the trends in the interaction energies and the NBO charge transfer. The interaction of porphyrin film with VOC gas is determined by the metal atom site via the interaction of the π electrons and the free electrons of the metal atom in porphyrin with the electrons of a gas molecule.[5] Therefore, electron transfer from the metal atom in porphyrin to an oxygen atom of the VOC molecule occurs when MgTPP/ZnTPP are in contact with the VOC molecule. The interaction energy at this site depends on the chemical properties of the central metal atom, such as electronegativity and spin state.

Overall, the DFT calculations show a clear difference of the molecular interaction nature with VOC between MgTPP and ZnTPP. The annealed MgTPP shows higher responses to methanol than the as spin-coated ZnTPP films in both experimental and computational results. In addition, the annealed MgTPP film with a microcrystalline structure, as evident from the AFM and XRD results, produces higher methanol response than the as spin-coated MgTPP films, whereas the opposite trend has been observed for ZnTPP. In general, strong gas-sensing response is to be expected from films with smaller grain sizes because of a higher surface area. The result of the MgTPP films seems initially to contradict the common sense. However, since the interactions of porphyrin and VOC molecules should occur via the charge transfer process. On one porphyrin semiconductive micro-crystal, one interacting VOC molecule can induce optical absorption change to the whole crystal, which may lead to the enhanced sensitivity. Meanwhile, for the ZnTPP, the as spin-coated films exhibit a better sensitivity. This may be possibly explained by structural changes induced by solvent vapor, which has been observed in the case of zinc phthalocyanine.[18]

4. Conclusion

MgTPP and ZnTPP spin coated thin films have been fabricated as optical gas sensors and applied to classify many types of VOCs under an artificial nose setup. The sensing response of the porphyrin molecules to vapor molecules was monitored by changes in the optical absorbance. MgTPP and ZnTPP thin films presented strong sensing signals with methanol and Thai whisky, respectively. In addition, the computational results were compared with experiment results, which confirm that, amongst methanol, ethanol and iso-propanol, MgTPP yields the highest interaction energy with methanol at the same concentration of alcohol vapor. XRD confirms that crystallization enhanced by thermal annealing of the MgTPP film helps improve the sensing response. Based on the PCA pattern recognition technique, both MgTPP and ZnTPP films can be successfully applied to discriminate three types of alcohols and Thai beverages.

RESEARCH ARTICLE

Acknowledgments: A research career development grant from the Thailand Research Fund to TK and a CHE-Ph.D.-SW-INV scholarship from the Commission of Higher Education to SK are acknowledged. We express our gratitude to Dr. Radchada Buntem for provision of ZnTPP. This research was supported by Mahidol University and the National Science and Technology Agency.

References and Notes

1. B. Wang, X. Zuo, Y. Q. Wu, and Z. M. Chem, *Sens. Actuators, B* 125, 268 (**2007**).
2. M. Campbell, Sensor System for Environmental Monitoring, Blackie Academic and Professional, London (**1997**), Vol. 1.
3. D. Manno, G. Micocci, A. Serra, A. Tepore, L. Valli, and D. P. Arnold, *Sens. Actuators, B* 57, 179 (**1999**).
4. P. Montmeat, S. Madonia, E. Pasquinet, L. Hairault, C. P. Gros, J. M. Barbe, and R. Guilard, *Proceeding of IEEE Sensors Journal* 5, 174 (**2005**).
5. A. A. Umar, M. M. Salleh, and M. Yahaya, *Sens. Actuators, B* 85, 191 (**2002**).
6. S. Uttiya, S. Pratontep, W. Bhanthumnavin, R. Buntem, and T. Kerdcharoen, *Proceeding of the 2nd IEEE INEC* (**2008**), p. 618.
7. S. Kladsomboon, S. Pratontep, S. Uttiya, and T. Kerdcharoen, *Proceeding of the 2nd IEEE INEC* (**2008**), p. 585.
8. X. Zhang, Y. Zhang, and J. Jiang, *Spectrochim. Acta Part A* 61, 2576 (**2005**).
9. K. A. Nguyen and R. Pachter, *J. Chem. Phys.* 114, 10757 (**2001**).
10. M. J. Fernandez, J. L. Fontecha, I. Sayago, M. Leixandre, J. Lozano, J. Gutierrez, I. Gracia, C. Cane, and M. C. Horrillo, *Sens. Actuators, B* 127, 277 (**2007**).
11. S. Kladsomboon, S. Pratontep, S. Uttiya, and T. Kerdcharoen, *Proceeding of the 4th IEEE INEMs* (**2009**), p. 824.
12. C. Zhang and K. S. Suslick, *J. Agric. Food Chem.* 55, 237 (**2007**).
13. C. Wongchoosuka, A. Wisitsoraatb, A. Tuantranontb, and T. Kerdcharoen, *Sens. Actuators, B* 147, 392 (**2010**).
14. P. M. Oppeneer, P. M. Panchmatia, B. Sanyal, O. Eriksson, and Md. E. Ali, *Progress in Surface Science* 84, 18 (**2009**).
15. S. Uttiya, T. Kerdcharoen, S. Vatanayon, and S. Pratontep, *J. Korean Phys. Soc.* 52, 1575 (**2008**).
16. C. D. George, T. Richardson, M. E. Hofton, C. M. Vale, M. G. M. Neves, and J. A. S. Cavaleiro, *Matter Sci. Eng.* 8–9, 559 (**1999**).
17. M. M. El-Nahass, H. M. Zeyada, M. S. Aziz, and M. M. Makhlouf, *Spectrochim. Acta Part A* 61, 3026 (**2005**).
18. S. Uttiya, S. Kladsomboon, O. Chamlek, W. Suwannet, T. Osotchan, T. Kerdcharoen, M. Brinkmann, and S. Pratontep, *Springer Proceedings in Physics* 129, 211 (**2009**).

Received: 30 December 2009. Revised/Accepted: 30 August 2010.

RESEARCH ARTICLE